arXiv:hep-ph/9810348v1 13 Oct 1998

HD-TVP-98/02

Transition rates for $q\bar{q} \to \pi\pi\pi$ in a chiral model

D. S. Isert, S. P. Klevansky and P. Rehberg*
Institut für Theoretische Physik,
Philosophenweg 19, D-69120 Heidelberg, Germany

Abstract

We investigate the nature of transition rates for the hadronization process of $q\bar{q} \to \pi\pi\pi$ as opposed to the transition rates for $q\bar{q} \to \pi\pi$, within the Nambu–Jona-Lasinio model that has manifest chiral symmetry. Feynman diagrams appropriate to this process can be classified according to the expansion in the inverse number of colors $1/N_c$. Two of these types of graphs are seen to be either "s-like" or "t-like" in nature. A further graph that contains both s-like and t-like elements, and which is denoted as st-like, is also present. To describe such a process with two incoming and three outgoing particles, it is necessary to extend the number of Mandelstam invariants. It is convenient to introduce seven such variables, of which only five are independent. The cross section for two incoming particles to three outgoing particles is then reexpressed in integral form in terms of these invariants. As a function of $\sqrt{s}$, the final expression is reduced to an integral over the four remaining invariants. The limits of integration, which are now non-trivial, are also discussed. The transition rate for the explicit case of $u\bar{u} \to \pi^+\pi^-\pi^0$, is evaluated numerically, assuming non-chiral pions, $m_\pi = 135$MeV. The rate for three pion production is found to be of the same order of magnitude as for two pion production, making this a non-negligible contribution to hadronization.

*Current address: SUBATECH, Laboratoire de Physique Subatomique et des Technologies Associées UMR, Université de Nantes, IN2P3/CNRS, Ecole des Mines de Nantes 4 Rue Alfred Kastler, F-44070 Nantes Cedex 03, France.

I. INTRODUCTION

Nonequilibrium formulations of field theories are in a stage of development at present. Their study is essential for ultimately constructing a solid theoretical basis for the transport codes that are used according to various models for the simulation of heavy-ion collisions. One such attempt that is still in its early stages investigates the nonequilibrium formulation of a *chiral* theory, the Nambu–Jona-Lasinio (NJL) model [1,2]. From practical experience, one assumes that a collision term of the associated semi-classical limit will be Boltzmann-like in form, and this has been demonstrated explicitly [3]. In particular, a full calculation that includes mesonic degrees of freedom must also contain not only quark-quark and quark-antiquark scattering cross-sections on the partonic level, but also the hadronization processes $q\bar{q} \to MM'$ and their dissolution, where M represents a mesonic state. Cross-sections for these processes in SU(3) have already been calculated and are given elsewhere [4].

Processes such as those described in the last paragraph are binary in nature. On the other hand, there are numerous other processes that may occur and which increase the total number of particles. While binary collisions lead to thermal equilibrium, other multiparticle collisions may also be required to attain chemical equilibrium. In particular, the simplest possible further kind of collision would be one that increases the number of particles, such as that of $q\bar{q} \to MM'M''$. Such a process should also rightly enter into the collision dynamics. If one had some knowledge of the magnitude of such processes, one would at least know whether multiparticle production in transport models could be expected to play an important role or not. In particular, one imagines that multiparticle hadronization processes such as the type just mentioned could be particularly important for the Goldstone bosons, the pions, since they are massless in the chiral limit, and are light in any event. Since pions are the dominant degree of freedom in the late phase of heavy-ion collisions, being produced copiously, it is essential to study their role. The purpose of this paper is thus to examine the cross-section for processes of the kind $q\bar{q} \to \pi\pi\pi$, where two particles enter the interaction region, while three are emitted. A direct numerical calculation is performed specifically for the case $u\bar{u} \to \pi^+\pi^-\pi^0$. This specific example has been chosen because the hadronization channel into two mesons

$u\bar{u} \to \pi^+\pi^-$ has already been calculated and has been shown to dominate over the other possible existing two pseudoscalar emission channels that include $u\bar{u} \to \pi^0\pi^0$, K^+K^- and $\pi^0\eta$ [4].

The chiral model underpinning our calculation is the NJL model, in which the SU(2) version is used. While this model has several shortcomings, specifically that it does not confine, it gives an excellent description of the mesonic and baryonic sectors [2]. In using this model, one is able to obtain a self-consistent description within a chiral theory, which ultimately may be used in developing a self-consistent transport theory that in turn is based purely on this chiral Lagrangian [3,5,6].

As a guide to determining the most relevant diagrams, the expansion in the inverse number of colors $1/N_c$ is used [7,8]. Within the same order of $1/N_c$, there are three types of diagrams, an s-like, a t-like, and a mixed so-called st-like graph. We find expressions for the invariant amplitudes in all three cases, and apply this to a calculation of the transition rates specifically for the process $u\bar{u} \to \pi^+\pi^-\pi^0$. Since there are many terms that contribute to each channel, we investigate all channels first separately, and find that the st-like channel is at least an order of magnitude larger than the s-like and t-like graphs. That is to say, within the $1/N_c$ ordering, there appears to be a subordering that dictates that one (or more) graphs are in fact dominant. In retrospect, one can give *heuristic* arguments why the particular st-like graph should in fact dominate. This particular graph contains the most divergent functions, since it contains a fermion loop with three propagators. The s-like graph by contrast contains a fermion loop with four propagators. In fact, such an ordering of terms within one specific class of diagrams that superficially are all of the same order in $1/N_c$ *rather* according to the degree of divergence of each graph was proposed long ago in Ref. [9]. The calculation in this paper thus serves also in part to validate *a posteriori* that this ordering correctly assesses the importance of each term. In Ref. [9], convergent terms were regarded as being secondary, while the leading behavior was determined solely by the divergent terms. In a further calculation of the pion radius [10], it has also been seen that the leading logarithmic contribution that is in accord with the well-known results of sigma models and chiral perturbation theory, is also due to the most divergent graph of the many available to the same order in the $1/N_c$ expansion when calculated in the NJL model. This is so because this graph naturally corresponds to the pion loop diagram that has been

known to give rise to the chiral logarithm in so many other models or theories, see for example Refs. [11–13]. Note that in Ref. [10], however, no explicit calculations of the remaining terms was undertaken.

In our numerical calculation of the transition rate that was carried out using a Monte Carlo procedure, we find that the st-like channel has the same order of magnitude for the production rate of $u\bar{u} \to \pi^+\pi^-\pi^0$ as is found for the dominant two particle production rate $u\bar{u} \to \pi^+\pi^-$ [4]. As such, it appears to give a nonnegligible contribution to the production cross-section for three pions and cannot be ignored in hadronization programs at low energies.

An essential feature of the calculation is the construction of the cross-section for the process of two incoming to three outgoing states, $a + b \to c + d + e$. To this end, we introduce extended Mandelstam-like variables that will be denoted as s, t, u, v, w, x and y, and we reexpress the cross-section in terms of these variables. The invariant amplitude, which is given by the relevant Feynman graphs is most easily expressible in terms of these extended variables [1]. Although this section of our work is performed for the case of incoming quarks and outgoing pions, and has thus the restriction $p_1^2 = p_2^2 = m^2$ and $p_3^2 = p_4^2 = p_5^2 = m_\pi^2$, the kinematics are otherwise unrestricted so that the generalization to other arbitrary three body processes is obvious.

This paper is organised as follows. In Section II, we evaluate the invariant amplitude for two arbitrary incoming quark flavors and outgoing mesonic states. In Section III, we discuss the kinematics of the process $a + b \to c + d + e$ and write the cross-section for this process in terms of extended Mandelstam-like variables. In Section IV, we calculate the cross-section for $u\bar{u} \to \pi^+\pi^-\pi^0$, and present our numerical results. We summarize and conclude in Section V.

II. HADRONIZATION INTO THREE PIONS.

In this section, we discuss the processes that lead to three pion production, governed by the SU(2) Nambu–Jona-Lasinio Lagrangian density

[1] Other choices are also possible [14]. The variables chosen here however, arise naturally when one examines the possible t-channel processes.

$$\mathcal{L} = \bar{\psi}(i\,\partial\!\!\!/ - m_0)\psi + G[(\bar{\psi}\psi)^2 + (\bar{\psi} i\gamma_5 \vec{\tau}\psi)^2] \ . \tag{2.1}$$

Here $m_0^u = m_0^d = m_0$ is the current quark mass for u and d quarks and G is a dimensionful coupling strength, $[G] = [\mathrm{MeV}]^{-2}$. There are several detailed reviews of this model in the literature, see for example Refs. [2]. The reader is referred to these references for a derivation of the gap equation that determines the constituent quark mass

$$m = m_0 + 2iGN_cN_f \int \frac{d^4p}{(2\pi)^4} \mathrm{tr} S(p) \tag{2.2}$$

with $S(p)^{-1} = \not{p} - m$ as well as for obtaining the pseudoscalar and scalar meson masses via the condition

$$1 - 2G\Pi_{S,PS}(k^2)|_{m_\sigma^2, m_\pi^2} = 0, \tag{2.3}$$

where the scalar and pseudoscalar polarization functions are defined in the usual way as

$$\Pi_{PS}(k^2) = -iN_c \mathrm{tr}_f(T_i T_f) \int \frac{d^4p}{(2\pi)^4} \frac{(-\not{p} + m)(\not{p} + \not{k} + m)}{[p^2 - m^2][(p+k)^2 - m^2]} \tag{2.4}$$

$$\Pi_S(k^2) = iN_c \int \frac{d^4p}{(2\pi)^4} \frac{(\not{p} + m)(\not{p} + \not{k} + m)}{[p^2 - m^2][(p+k)^2 - m^2]} \tag{2.5}$$

with T_i an isospin operator $T_3 = \tau_3$ and $T_\pm = (\tau_1 \pm i\tau_2)/\sqrt{2}$.

Using the concept now that one can construct the Feynman diagrams for any process involving quarks, antiquarks and mesons, one can classify the graphs that contribute to hadronization. In the case that one has hadronization into *two* particles, this is given in the standard fashion according to s channel, t channel and u channel graphs, as is shown in Fig. 1. Here s, t and u are the usual Mandelstam variables, $s = (p_1 + p_2)^2$, $t = (p_1 - p_3)^2$ and $u = (p_1 - p_4)^2$. From energy-momentum conservation, $p_1 + p_2 = p_3 + p_4$, one has the additional constraint

$$s + t + u = 2m^2 + 2m_\pi^2. \tag{2.6}$$

These amplitudes and their resulting cross-sections have been discussed in detail in Ref. [4]. Note that the set of graphs is chosen to be leading in the $1/N_c$ expansion [7,8]. That the s, t and u channels are of the same order lies in the fact that meson propagators (in the pionic channel) are constructed as intermediate states

into quark-antiquark scattering amplitudes. These quark-antiquark scattering amplitudes contribute as $g^2_{\pi qq}/m^2_\pi \sim 1/N_c$, as has been explicitly shown in Ref. [8], for example. A fermionic loop on the other hand brings a contribution of order $\sim N_c$.

Generic diagrams that we can construct for two incoming quarks and three outgoing mesons are shown in Fig. 2(a)-(c). We note that in direct analogy to the graphs of Fig. 1, we can order the hadronization graphs of Figs. 2(a) and 2(b) as being *s-like* or *t-like*. Figure 2(c) fits into neither category and we thus denote it as *st-like*. As has already been stated, the graphs of Fig. 2 are generic: the full set of diagrams is obtained for Figs. 2(a) and 2(b) by permuting the outgoing momenta. There are $3! = 6$ ways of doing this. Whether all 6 diagrams in each case contribute to a process or not is then determined by the flavor factors of the individual incoming quarks in question. In Fig. 2(c), four cases arise on noting that the vertex for two particle production can be attached either to the incoming (top or bottom) quark or antiquark line, and the sense of the line in the quark loop can be clockwise or anticlockwise. The single emanating meson line can also take on any of the final state momenta, leading to a further permutation of these three possibilities. Exact combinations again depend on the flavors of the vertices in question.

For two incoming states to three outgoing states, it is useful to define the extended Mandelstam-like variables,

$$\begin{aligned} s &= (p_1 + p_2)^2 \\ t &= (p_1 - p_3)^2 \\ u &= (p_1 - p_4)^2 \\ v &= (p_1 - p_5)^2 \\ w &= (p_1 - p_3 - p_4)^2 = (p_2 - p_5)^2 \\ x &= (p_1 - p_4 - p_5)^2 = (p_2 - p_3)^2 \\ y &= (p_1 - p_3 - p_5)^2 = (p_2 - p_4)^2, \end{aligned} \tag{2.7}$$

where the last relations follow from energy-momentum conservation, $p_1 + p_2 = p_3 + p_4 + p_5$. Using, in addition, the restriction to quarks for the incoming states,

$$p_1^2 = p_2^2 = m^2 \tag{2.8}$$

and pions for the outgoing states,

$$p_3^2 = p_4^2 = p_5^2 = m_\pi^2, \tag{2.9}$$

we find

$$s + t + u + v = 3m^2 + 3m_\pi^2 \tag{2.10}$$

and

$$s + w + x + y = 3m^2 + 3m_\pi^2, \tag{2.11}$$

in analogy to Eq.(2.6).

In what follows, in our analysis of the s-like and t-like graphs, the products p_1p_2, p_1p_3 and so forth, occur. These are simply related to the extended Mandelstam variables via, e. g.,

$$\begin{aligned} p_1 \cdot p_2 &= \frac{1}{2}(s - 2m^2) \\ p_1 \cdot p_3 &= -\frac{1}{2}(t - m^2 - m_\pi^2). \end{aligned} \tag{2.12}$$

We do not explicitly rewrite our expressions in terms of these variables: the numerical program makes a direct translation. In contrast to this, the t-like channel amplitudes are most simply written directly in terms of these variables and we thus use them explicitly from the start.

A. s-like channel

In this section, we discuss the s-like channel diagram involving an intermediate scalar or pseudoscalar meson. One of the six possible ways of distributing the momenta is shown in Fig. 3. We shall assume that the final state always contains three pseudoscalar particles. In this case, if the intermediate meson is a scalar, the scattering amplitude, vanishes,

$$-i\mathcal{M}_\sigma(p_3, p_4, p_5) = 0. \tag{2.13}$$

This must be so on general grounds, since the parity of the final state is negative, in contrast to the positive parity of the intermediate state. This can also be validated by direct calculation.

We thus require Fig. 3 calculated with the pion in the intermediate state. We examine this single diagram first with the momenta as indicated in the figure. Using an obvious notation, this is

$$-i\mathcal{M}_\pi(p_3,p_4,p_5) = \bar{v}_2 i\gamma_5 T_j u_1 \delta_{c_1c_2} \frac{2iG}{1-2G\Pi_{PS}(k^2)} (ig_{\pi qq})^3 A_{\pi\pi\pi\pi}(p_3,p_4,p_5), \tag{2.14}$$

where the four pion vertex is given as

$$\begin{aligned} &A_{\pi\pi\pi\pi}(p_3,p_4,p_5) = \\ &-\mathrm{Tr}\int \frac{d^4q}{(2\pi)^4} i\gamma_5 T_k iS(q-k) i\gamma_5 T_5 iS(q-p_3-p_4) i\gamma_5 T_4 iS(q-p_3) i\gamma_5 T_3 iS(q). \end{aligned} \tag{2.15}$$

In this expression, $\mathrm{Tr} = \mathrm{tr}_\gamma \mathrm{tr}_f \mathrm{tr}_c$ sums over all degrees of freedom, and T_i is an appropriate flavor operator. Color appears trivially as shown by the δ-function in Eq.(2.14). Inserting the single particle propagator leads to the form

$$\begin{aligned} &A_{\pi\pi\pi\pi}(p_3,p_4,p_5) = -N_c N_f^{(345k)} \times \\ &\int \frac{d^4q}{(2\pi)^4} \frac{\mathrm{tr}_\gamma[(-\not{q}+\not{k}+m)(\not{q}-\not{p}_3-\not{p}_4+m)(-\not{q}+\not{p}_3+m)(\not{q}+m)]}{(q^2-m^2)[(q-p_3)^2-m^2][(q-p_3-p_4)^2-m^2][(q-k)^2-m^2]} \end{aligned} \tag{2.16}$$

and the flavor factor is abbreviated as $N_f^{(345k)} = \mathrm{tr}_f(T_k T_5 T_4 T_3)$. The flavor factor to be associated with the complete s-like channel is then

$$f_s^{(345)} = N_f^{(j)} N_f^{(345k)}, \tag{2.17}$$

where $N_f^{(j)} = \bar{q} T_j q$ arises from the choice of incoming quark and antiquark. Directly performing the spinor trace leads to the expression

$$\begin{aligned} &A_{\pi\pi\pi\pi}(p_3,p_4,p_5) = -2N_c N_f^{(345k)} [(-k^2 p_3 p_4 - k p_4 m_\pi^2) I_4(k, p_3+p_4, p_3, 0) \\ &+2(kp_3) p_4 \tilde{I}_4(k, p_3+p_4, p_3, 0) + p_3 p_4 I_3(p_3+p_4, p_3, 0) \\ &+(kp_4 - k^2) I_3(p_3+p_4, k, 0) + (kp_4 - p_3 p_4 - m_\pi^2) I_3(p_3, p_3+p_4, k) \\ &+I_2(p_3+p_4, 0) + I_2(k, p_3), \end{aligned} \tag{2.18}$$

where

$$I_n(a_1,\ldots,a_n) = \int \frac{d^4q}{(2\pi)^4} \frac{1}{[(q-a_1)^2-m^2]\ldots[(q-a_n)^2-m^2]} \tag{2.19}$$

and $\tilde{I}_4$ is defined as

$$\tilde{I}_4(a_1,\ldots,a_4)^\mu = \int \frac{d^4q}{(2\pi)^4} \frac{q^\mu}{[(q-a_1)^2-m^2]\ldots[(q-a_4)^2-m^2]}. \tag{2.20}$$

This latter integral, in combination with an external momentum can be reduced to a linear combination of the I_n. These functions are listed in Appendix A.

The diagram of Fig. 3 represents one of the six possibilities of ordering the external momenta. Another of these is obtained by reversing the arrows on the internal loop of the vertex, as shown in Fig. 4. Translation of this Feynman diagram gives

$$\begin{aligned} &A_{\pi\pi\pi\pi}(p_5,p_4,p_3) = \\ &-\mathrm{Tr}\int \frac{d^4q}{(2\pi)^4} i\gamma_5 T_k iS(-q) i\gamma_5 T_3 iS(p_3-q) i\gamma_5 T_4 iS(p_3+p_4-q) i\gamma_5 T_5 iS(k-q). \end{aligned} \tag{2.21}$$

Some algebra is required to evaluate the traces. The spinor trace can be shown to be equivalent to that required for Eq.(2.16). In addition, the flavor traces are equal,

$$N_f^{(543k)} = N_f^{(345k)}, \tag{2.22}$$

so that

$$A_{\pi\pi\pi\pi}(p_5,p_4,p_3) = A_{\pi\pi\pi\pi}(p_3,p_4,p_5). \tag{2.23}$$

This is a general feature when reversing the loop momenta for the diagrams required here. Hence the combination of six terms for the s-like channel reduces to a calculation of 2 times three terms. The remaining two "crossed" s-like graphs for the vertices are shown in Fig. 5. The associated vertex functions are $A_{\pi\pi\pi\pi}(p_4,p_5,p_3)$ and $A_{\pi\pi\pi\pi}(p_5,p_4,p_3)$, which can be obtained from Eq.(2.18) on suitably interchanging the arguments.

One may finally construct the scattering amplitude for the s-like channel as

$$-i\mathcal{M}_\pi^{s-\mathrm{like}} = -2i[\mathcal{M}_\pi(p_3,p_4,p_5) + \mathcal{M}_\pi(p_4,p_5,p_3) + \mathcal{M}_\pi(p_5,p_3,p_4)], \tag{2.24}$$

where

$$-i\mathcal{M}_\pi(p_a,p_b,p_c) = \bar{v}_2 i\gamma_5 u_1 \delta_{c_1,c_2} \frac{2G}{1-2G\Pi_{PS}(k^2)} g_{\pi qq}^3 N_f^{(j)} A_{\pi\pi\pi\pi}(p_a,p_b,p_c). \quad (2.25)$$

Since $\Pi_{PS}(k^2)$ and $g_{\pi qq}$ can also be expressed through the integrals I_n,

$$-i\Pi_{PS}(k^2) = 4N_c(2I_1(0) - k^2 I_2(0,-k)) \quad (2.26)$$

$$g_{\pi qq}^{-2} = -4iN_c I_2(0,-k), \quad (2.27)$$

a direct evaluation of this quantity depends only on the evaluation of the integrals I_n, see Appendix A.

For the purpose of obtaining a scattering cross-section, the absolute value of the scattering amplitude is averaged over initial states and summed over the final ones. Since $\sum_{s_1,s_2} |\bar{v}_2 i\gamma_5 u_1|^2 = 2s$, it follows that

$$\overline{|\mathcal{M}_\pi(p_a,p_b,p_c)|^2} = \frac{2G^2 g_{\pi qq}^6 (N_f^{(j)})^2 s}{N_c} \frac{|A_{\pi\pi\pi\pi}(p_a,p_b,p_c)|^2}{|1-2G\Pi_{PS}(k^2)|^2} \quad (2.28)$$

from which $\overline{|\mathcal{M}_\pi^{s-\text{like}}|^2}$ can be constructed.

B. t-like channel

The six possible t-like channel graphs are shown in Fig. 6, together with our labelling of each process. As an example, we calculate one of these diagrams explicitly. Considering the $t-w$ channel depicted in Fig. 6a, one finds

$$-i\mathcal{M}^{(t,w)} = \bar{v}_2 i g_{\pi qq} i\gamma_5 T_5 i S(p_1-p_3-p_4) i g_{\pi qq} i\gamma_5 T_4 i S(p_1-p_3) i g_{\pi qq} i\gamma_5 T_3 u_1 \delta_{c_1 c_2}, \quad (2.29)$$

and therefore the absolute value of the scattering amplitude averaged over initial states and summed over the final ones follows as

$$\begin{aligned}\overline{|\mathcal{M}^{(t,w)}|^2} = \frac{1}{4N_c^2} \sum_{s_1 s_2} \frac{-f_{t,w}^2 g_{\pi qq}^6 N_c}{(t-m^2)^2(w-m^2)^2} \mathrm{tr}[&v_2\bar{v}_2\gamma_5(\not{p}_1 - \not{p}_3 - \not{p}_4 + m)\gamma_5 \\ &\cdot(\not{p}_1 - \not{p}_3 + m)\gamma_5 u_1\bar{u}_1\gamma_5(\not{p}_1 - \not{p}_3 + m)\gamma_5(\not{p}_1 - \not{p}_3 - \not{p}_4 + m)\gamma_5].\end{aligned} \quad (2.30)$$

The trace over flavor matrices has been abbreviated as $f_{t,w} = \mathrm{tr}(T_5 T_4 T_3)$. After some tedious algebra for evaluating the spinor trace, one arrives at the relatively simple form

$$\overline{|\mathcal{M}^{(t,w)}|^2} = \frac{f_{t,w}^2 g_{\pi qq}^6}{2N_c}\left[\frac{-1}{t-m^2}\left(1+\frac{x-u}{w-m^2}\right)+\frac{m_\pi^6}{(t-m^2)^2(w-m^2)^2}\right.$$
$$\left.+\frac{m_\pi^2}{(t-m^2)(w-m^2)}\left(2-\frac{y-m^2}{t-m^2}-\frac{u-m^2}{w-m^2}\right)\right], \tag{2.31}$$

in which the invariants t, u, x, y and w occur. Completely analogous calculations lead to the expressions for the remaining five channels, $\overline{|\mathcal{M}^{(u,x)}|^2}$, $\overline{|\mathcal{M}^{(v,y)}|^2}$, $\overline{|\mathcal{M}^{(t,y)}|^2}$, $\overline{|\mathcal{M}^{(u,w)}|^2}$ and $\overline{|\mathcal{M}^{(v,x)}|^2}$. These can be obtained directly from Eq.(2.31) by making an appropriate variable substitution. To obtain $\overline{|\mathcal{M}^{(u,x)}|^2}$, one makes the replacement

$$\begin{aligned} t &\to u \to v \\ w &\to x \to y \to w \end{aligned} \tag{2.32}$$

in Eq.(2.31), that follows on examining the momentum dependence of Fig. 6b in comparison with that of Fig. 6a. Similarly, the expression for $\overline{|\mathcal{M}^{(v,y)}|^2}$ follows from Eq.(2.31) on substituting

$$\begin{aligned} t &\to v \qquad u \to t \\ w &\to y \to x \to w, \end{aligned} \tag{2.33}$$

while $\overline{|\mathcal{M}^{(t,y)}|^2}$ is obtained on writing

$$\begin{aligned} t &\to t \qquad x \to x \\ u &\to v \qquad w \leftrightarrow y, \end{aligned} \tag{2.34}$$

$\overline{|\mathcal{M}^{(u,w)}|^2}$ from Eq.(2.31) on writing

$$\begin{aligned} t &\leftrightarrow u \\ w &\to w \qquad x \leftrightarrow y, \end{aligned} \tag{2.35}$$

and $\overline{|\mathcal{M}^{(v,x)}|^2}$ from Eq.(2.31) on writing

$$\begin{aligned} t &\to v \qquad u \to u \\ w &\leftrightarrow x \qquad y \to y. \end{aligned} \tag{2.36}$$

All expressions have relatively simple analytic forms. One notices that in the chiral limit, $m_\pi = 0$, they simplify dramatically.

C. *st*-like channel

The *st*-like channel of Fig. 2(c) is evaluated by separating the vertex for two meson production from that of single meson production. This diagram is thus subdivided into two pieces, the first containing the quark-qntiquark scattering amplitude that is mediated by an exchanged meson connected with a quark loop as indicated in Fig. 7. Implicit in this diagram is that both the clockwise and counterclockwise senses in the fermion loop are to be evaluated. Since we will regard pions the final state, it follows from parity conservation that the intermediate mesonic state must be a scalar. In this case, this is then taken to be the σ meson. Since the two flavor NJL model is considered here, the two pions that emerge from this vertex must be charge neutral. Translating Fig. 7, one has

$$A_{\sigma\pi\pi}(p) = iD_S(p^2)(ig_{\pi qq})^2(-2N_c)\mathrm{tr}_f T_3 T_4 \\ \times \int \frac{d^4q}{(2\pi)^4}\mathrm{tr}_\gamma[i\gamma_5 iS(q)i\gamma_5 iS(q+p_3)iS(q-p_4)]. \tag{2.37}$$

The factor 2 arises from considering both senses of the fermion loop, and again tr_γ is the trace on Dirac indices. In this expression, $D_S(p^2)$ is the quark-quark scattering amplitude in the scalar σ channel, i.e.

$$D_S(p^2) = \frac{2G}{1-2G\Pi_S(p^2)}. \tag{2.38}$$

In principle, the exchange of the σ meson within the model as required here, involves a complex function, since the σ is a resonance. It is, however, only weakly unbound, with $m_\sigma^2 \simeq 4m^2 + m_\pi^2$, and consequently here only principle values of the integrals I_n entering into the evaluation of the irreducible polarization $\Pi_S(p^2)$ is used.

By making the substitution $q \to -q$ in the second integral of Eq.(2.37) and performing the trace, one arrives at the following expression for this function,

$$A_{\sigma\pi\pi}(p) = 16mN_c g_{\pi qq}^2 D_S(p^2)[I_2(p_3,-p_4) + p_3\cdot p_4 I_3(0,p_3,-p_4)]. \tag{2.39}$$

This graph is then embedded into the hadronization graph of Fig. 2(c). Attaching the vertex $A_{\sigma\pi\pi}$ to both the incoming quark line, as was drawn originally in Fig. 2(c) plus the incoming antiquark line, which is also a required configuration, leads to two terms,

$$\mathcal{M}^{(st)} = \bar{v}(p_2)[i\gamma^5 T i g_{\pi qq}\frac{i(\not{p}_5 - \not{p}_2 + m)}{(p_5 - p_2)^2 - m^2}A_{\sigma\pi\pi}(p_3 + p_4)$$
$$+ A_{\sigma\pi\pi}(p_3 + p_4)\frac{i(\not{p}_1 - \not{p}_5 + m)}{(p_1 - p_5)^2 + m^2}i\gamma^5 T i g_{\pi qq}]u(p_1)$$
$$= \mathcal{M}_1^{(st)} + \mathcal{M}_2^{(st)}. \tag{2.40}$$

The averaged transition matrix element then follows as

$$\overline{|\mathcal{M}^{(st)}|^2} = \frac{1}{2N_n}g_{\pi qq}^2|A_{\sigma\pi\pi}(p_3 + p_4)|^2\left\{\frac{1}{w - m^2} + \frac{1}{v - m^2}\right\}^2$$
$$\times \{m_\pi^2(4m^2 - s) + (v - m^2 - m_\pi^2)(w - m^2 - m_\pi^2)\}. \tag{2.41}$$

Since p_5 is the momentum of the pion line that is attached singly, we use the notation $\mathcal{M}^{(st)}(p_5)$ to denote this fact.

D. Full scattering amplitude

The full scattering amplitude is comprised of all s-like, t-like and st-like contributions, *i.e.*

$$\mathcal{M} = 2\mathcal{M}_\pi(p_3, p_4, p_5) + 2\mathcal{M}_\pi(p_4, p_5, p_3) + 2\mathcal{M}_\pi(p_5, p_3, p_4)$$
$$+ \mathcal{M}^{(t,w)} + \mathcal{M}^{(u,x)} + \mathcal{M}^{(v,y)} + \mathcal{M}^{(t,y)} + \mathcal{M}^{(u,w)} + \mathcal{M}^{(v,x)}$$
$$+ \mathcal{M}^{(st)}(p_3) + \mathcal{M}^{(st)}(p_4) + \mathcal{M}^{(st)}(p_5). \tag{2.42}$$

As such, the cross-section requires not only the averaged terms that were given in Eqs.(2.28) and (2.31) - (2.36), but also mixed terms that arise on building the modulus. There are many of these and we have listed some of them in Appendix B.

III. THE SCATTERING CROSS-SECTION FOR $q\bar{q} \to \pi\pi\pi$ IN TERMS OF EXTENDED MANDELSTAM-LIKE VARIABLES

A. Cross section

The notion of relativistic invariance is an important calculational guide in evaluating matrix elements. As such, it is particularly useful to express the integrated cross section in terms of relativistic invariants only. To do this in the case when two particles are incident and two are exiting is a standard textbook exercise, see for

example [15]. However, when three particles are involved in the exit channel, as is the case here, this becomes somewhat more complex, and we are required to derive a formal expression. The only restriction that occurs in our derivation is that the incident particles with momenta p_1 and p_2 refer to particles with the same mass, *i.e.* $p_1^2 = p_2^2 = m^2$, while the exiting particles with momenta p_3, p_4, and p_5 also are bound by the constraint $p_3^2 = p_4^2 = p_5^2 = m_\pi^2$. The generalization to arbitrary mass particles in describing the reaction of $a + b \to c + d + e$ is obvious.

Starting from the definition of the cross section

$$\sigma = \int \frac{(2\pi)^4 \delta^{(4)}(p_3 + p_4 + p_5 - p_1 - p_2)\, \overline{|\mathcal{M}(p_1, p_2, p_3, p_4, p_5)|^2}}{|\vec{v}_{rel}| 2E_1 2E_2} \times \frac{d^3p_3}{(2\pi)^3 2E_3} \frac{d^3p_4}{(2\pi)^3 2E_4} \frac{d^3p_5}{(2\pi)^3 2E_5} \tag{3.1}$$

and the definition of the extended Mandelstam-like variables of Eq.(2.7), we use the identity

$$\int dp_5^0\, \Theta(p_5^0)\, \delta(p_5^2 - m_\pi^2)\, 2p_5^0 = 1 \tag{3.2}$$

and perform the p_5 integration, giving

$$\sigma = \int \frac{\overline{|\mathcal{M}(s,t,u,v,w,x,y)|^2}}{(2\pi)^5\, |\vec{v}_{rel}| 2E_1 2E_2} \frac{d^3p_3}{2E_3} \frac{d^3p_4}{2E_4}\, \delta((p_1 + p_2 - p_3 - p_4)^2 - m_\pi^2) \times\ \Theta(p_1^0 + p_2^0 - p_3^0 - p_4^0). \tag{3.3}$$

From energy conservation, the argument of the Θ function can be evaluated to be $p_1^0 + p_2^0 - p_3^0 - p_4^0 = E_1 + E_2 - E_3 - E_4 = E_5 > 0$, so that the Θ function takes the value 1. The argument of the δ function can be reexpressed in terms of the extended Mandelstam-like variables either as

$$(p_1 + p_2 - p_3 - p_4)^2 - m_\pi^2 = s + w + x + y - 3m^2 - 3m_\pi^2 \tag{3.4}$$

or as

$$(p_1 + p_2 - p_3 - p_4)^2 - m_\pi^2 = s + t + u + v - 3m^2 - 3m_\pi^2, \tag{3.5}$$

and the fact that the δ function contributes only when the right hand side of Eqs.(3.4) or (3.5) is zero leads to the energy momentum relations already stated in Eqs.(2.10) or (2.11).

As a consequence of their definitions in Eq.(2.7), the variables s, t, u and w are unaffected by the p_5 integration. On the other hand, v, x and y are altered,

$$\begin{aligned} v &= (p_1 - p_5)^2 \qquad \to (p_2 - p_3 - p_4)^2 \\ x &= (p_1 - p_4 - p_5)^2 \to (p_2 - p_3)^2 \\ y &= (p_1 - p_3 - p_5)^2 \to (p_2 - p_4)^2. \end{aligned} \tag{3.6}$$

The next task lies in transforming the element of integration and determining the appropriate Jacobian. To this end, we denote $\theta_{3,4}$ as being the angle between the vectors $\vec{p}_1$ and $\vec{p}_3$ or $\vec{p}_4$. Since we work in the c.m. reference frame, $\vec{p}_1$ and $\vec{p}_2$ lie in opposite directions so that the angle between $\vec{p}_2$ and $\vec{p}_3$ or $\vec{p}_4$ is $(\pi - \theta_{3,4})$. In addition, $|\vec{p}_1| = |\vec{p}_2|$, so that the extended Mandelstam-like variables of Eq.(2.7) take on the forms

$$t = m^2 + m_\pi^2 - 2E_1E_3 + 2|\vec{p}_1||\vec{p}_3|\cos\theta_3 \tag{3.7a}$$

$$u = m^2 + m_\pi^2 - 2E_1E_4 + 2|\vec{p}_1||\vec{p}_4|\cos\theta_4 \tag{3.7b}$$

$$\begin{aligned} v = {} & m^2 + 2m_\pi^2 - 2E_1E_3 - 2E_1E_4 + 2E_3E_4 \\ & -2|\vec{p}_1||\vec{p}_3|\cos\theta_3 - 2|\vec{p}_1||\vec{p}_4|\cos\theta_4 \\ & -2|\vec{p}_3||\vec{p}_4|(\sin\theta_3\sin\theta_4\cos(\varphi_4 - \varphi_3) + \cos\theta_3\cos\theta_4) \end{aligned} \tag{3.7c}$$

$$\begin{aligned} w = {} & m^2 + 2m_\pi^2 - 2E_1E_3 - 2E_1E_4 + 2E_3E_4 \\ & +2|\vec{p}_1||\vec{p}_3|\cos\theta_3 + 2|\vec{p}_1||\vec{p}_4|\cos\theta_4 \\ & -2|\vec{p}_3||\vec{p}_4|(\sin\theta_3\sin\theta_4\cos(\varphi_4 - \varphi_3) + \cos\theta_3\cos\theta_4) \end{aligned} \tag{3.7d}$$

$$x = m^2 + m_\pi^2 - 2E_1E_3 - 2|\vec{p}_1||\vec{p}_3|\cos\theta_3 \tag{3.7e}$$

$$y = m^2 + m_\pi^2 - 2E_1E_4 - 2|\vec{p}_1||\vec{p}_4|\cos\theta_4. \tag{3.7f}$$

For conciseness, we have used the abbreviation $E_{3,4}^2 = |\vec{p}_{3,4}|^2 + m_\pi^2$, but draw the attention of the reader to the fact that we consider $|\vec{p}_{3,4}|$ together with the angles as variables, and not $E_{3,4}$, althougth this would be equivalent. By contrast, E_1 and E_2 are fixed by the centre of mass condition, $E_1 = E_2 = \sqrt{s}/2$. Conversely the inverse transformation can be obtained. By adding and subtracting Eq.(3.7a) from Eq.(3.7e), one can easily find the determining equations for $|\vec{p}_3|$ and θ_3. A similar manipulation of Eqs.(3.7b) and (3.7f) yields those for $|\vec{p}_4|$ and θ_4. Having done this, Eqs.(3.7c) or (3.7d) can be easily solved for $\cos(\varphi_4 - \varphi_3)$. The exact form of this transformation is

$$t - x = 4|\vec{p}_1||\vec{p}_3|\cos\theta_3 \;\Rightarrow\; |\vec{p}_3|\cos\theta_3 = \frac{t-x}{4|\vec{p}_1|}, \tag{3.8a}$$

$$u - y = 4|\vec{p}_1||\vec{p}_4|\cos\theta_4 \;\Rightarrow\; |\vec{p}_4|\cos\theta_4 = \frac{u-y}{4|\vec{p}_1|}, \tag{3.8b}$$

$$t + x = 2m^2 + 2m_\pi^2 - 4E_1E_3 \;\Rightarrow\; E_3 = \frac{2m^2 + 2m_\pi^2 - t - x}{4E_1}, \tag{3.8c}$$

$$u + y = 2m^2 + 2m_\pi^2 - 4E_1E_4 \;\Rightarrow\; E_4 = \frac{2m^2 + 2m_\pi^2 - u - y}{4E_1}, \tag{3.8d}$$

while the expression for $\cos\varphi_{34}$ is

$$\cos\varphi_{34} = \frac{t + u - w - m^2 + 2E_3E_4 - 2|\vec{p}_3||\vec{p}_4|\cos\theta_3\cos\theta_4}{2|\vec{p}_3||\vec{p}_4|\sin\theta_3\sin\theta_4}. \tag{3.9}$$

Returning to the integrand in Eq.(3.3), one sees that it depends only on the extended Mandelstam-like variables, that in turn can be written in terms of $|\vec{p}_3|$, $|\vec{p}_4|$, θ_3, θ_4 and the difference $\varphi_{34} = \varphi_4 - \varphi_3$. Thus

$$\int d\varphi_3 d\varphi_4 = 2\pi \int d\varphi_{34}. \tag{3.10}$$

There are five independent integration variables, $|\vec{p}_3|$, $|\vec{p}_4|$, θ_3, θ_4 and φ_{34}. On the other hand, there are seven extended Mandelstam variables. As can be seen from Eqs.(3.7c) and (3.7d), both v and w are functions of the variable φ_{34}; we arbitrarily choose to discard v. In keeping with convention, the other unrelated variable is s, the square of the center of mass energy of the incoming particles. We thus are required to relate the multidimensional volume element in the variables $|\vec{p}_3|$, $|\vec{p}_4|$, θ_3, θ_4 and φ_{34} to the extended set t, u, w, x and y, which follows as

$$2|J|\, d|\vec{p}_3|\, d|\vec{p}_4|\, d\theta_3\, d\theta_4\, d\varphi_{34} = dt\; du\; dw\; dx\; dy, \tag{3.11}$$

where the factor 2 has been introduced together with the reduction of the integration region of φ_{34} from $[0, 2\pi]$ to $[0, \pi]$. After some calculation, one finds the Jacobian of the transformation to be

$$|J| = 128\,|\vec{p}_1|^2\,|\vec{p}_3|^3\,|\vec{p}_4|^3\,\sin^2\theta_3\,\sin^2\theta_4\,\frac{E_1^2}{E_3E_4}\,|\sin\varphi_{34}|. \tag{3.12}$$

Using the information from Eqs.(3.4) and (3.12), the cross section takes the form

$$\sigma = \int \frac{\overline{|\mathcal{M}'(s,t,u,w,x,y)|^2}}{(2\pi)^4\, 4|\vec{p}_1|\sqrt{s}}\,\delta(s + w + x + y - 3m^2 - 3m_\pi^2)$$
$$\times \frac{|\vec{p}_3|^2\,\sin\theta_3\,|\vec{p}_4|^2\,\sin\theta_4\,E_3\,E_4\,dt\,du\,dw\,dx\,dy}{2E_3\,2E_4\,256|\vec{p}_1|^2|\vec{p}_3|^3|\vec{p}_4|^3\sin^2\theta_3\,\sin^2\theta_4\,E_1^2\,|\sin\varphi_{34}|}, \tag{3.13}$$

$$\tag{3.14}$$

which can be written in a simpler form as

$$\sigma(s) = \frac{1}{64(2\pi)^4}\int dt\,du\,dw\,dx\,dy \frac{1}{N(s(s-4m^2))^{3/2}}\overline{|\mathcal{M}'(s,t,u,w,x,y)|^2}$$
$$\times \qquad \delta(s+w+x+y-3m^2-3m_\pi^2), \tag{3.15}$$

where use has been made of the relationship $4|\vec{p}_1|^2 = s - 4m^2$. In both Eqs.(3.14) and (3.15), the notation M' has been introduced to remind us that the variable v in the calculated matrix elements is to be replaced by $(-s-t-u+3m^2+3m_\pi^2)$ and the factor

$$N = 2|\vec{p}_3||\vec{p}_4|\sin\theta_3\sin\theta_4\sqrt{1-\cos^2\varphi_{34}} \tag{3.16}$$

has been abbreviated in the denominator. Clearly N must also be expressed in terms of the extended Mandelstam-like invariants. One finds the rather unwieldy expression

$$\begin{aligned}
N &= N(s,t,u,w,x,y) \\
&= \Bigg[\frac{-1}{4s(s-4m^2)}[(2m^2+2m_\pi^2)(t-x-u+y)+2ux-2ty]^2 \\
&\quad +m_\pi^2\left(\frac{(t-x)^2+(u-y)^2}{s-4m^2} - \frac{(2m^2+2m_\pi^2-t-x)^2+(2m^2+2m_\pi^2-u-y)^2}{s}\right) \\
&\quad -(t+u-w-m^2)^2+4m_\pi^4 \\
&\quad +(t+u-w-m^2)\left(\frac{(2m^2+2m_\pi^2-t-x)(2m^2+2m_\pi^2-u-y)}{s}\right. \\
&\quad \left.-\frac{(t-x)(u-y)}{s-4m^2}\right)\Bigg]^{1/2}.
\end{aligned} \tag{3.17}$$

In the chiral limit, this function simplifies somewhat.

As a final step, the integration on w can be performed and we obtain our final expression for the cross section:

$$\sigma(s) = \frac{1}{64(2\pi)^2}\int dt\,du\,dx\,dy\,\frac{\overline{|\mathcal{M}''(s,t,u,x,y)|^2}}{(s(s-4m^2))^{3/2}N(s,t,u,x,y)}, \tag{3.18}$$

which involves a fourfold integration. The notation M'' serves here to remind one that w has been integrated out, and is to be replaced by $(3m^2+3m_\pi^2-s-x-y)$ in these matrix elements. Using an obvious notation, the function

$$N(s,t,u,x,y) = N(s,t,u,w=3m^2+3m_\pi^2-s-x-y,x,y) \tag{3.19}$$

can be obtained from Eq.(3.17). This result generalizes the well-known form for the cross section for two incoming particles to two outgoing particles,

$$\sigma(s) = \int \frac{\overline{|\mathcal{M}'(s,t)|^2}}{16\pi s(s-4m^2)} dt \tag{3.20}$$

in which $\mathcal{M}'(s,t)$ denotes matrix elements $\mathcal{M}'(s,t) = \mathcal{M}(s,t,u = 2m^2+2m_\pi^2-s-t)$, for $q\bar{q} \to \pi\pi$ say.

B. Limits

In reactions of the type $a + b \to c + d$, for which the cross section of the form Eq.(3.20) holds, the determination of the limits of integration of the single variable t is simple: it is always related to one angular variable by virtue of its definition, and the minimum and maximum values of this angular variable lead to a minimum and maximum value of t respectively. For the case that is implicit in Eq.(3.20), a simple analytic form for t_{max} and t_{min} can be found. One has

$$t_{max} = m^2 + m_\pi^2 - \frac{s}{2} + \sqrt{s-4m^2}\sqrt{\frac{s}{4} - m_\pi^2} \tag{3.21}$$

and

$$t_{min} = m^2 + m_\pi^2 - \frac{s}{2} - \sqrt{s-4m^2}\sqrt{\frac{s}{4} - m_\pi^2} \tag{3.22}$$

for the case of different particles and

$$t_{min} = m^2 + m_\pi^2 - \frac{s}{2} \tag{3.23}$$

when there are identical particles in the final state.

By contrast, in our case where there are three outgoing particles in the final state, we have four integration variables t, u, x and y, whose ranges have to be determined, and which are laid fixed by the maximum and minimum values that these variables can take according to Eqs. (3.7a)-(3.7f) which are in turn set by the appropriate minimal and maximal values of the angular and energy variables that occur therein. For this reason, it is difficult to give simple expressions for these limits and we thus start by giving their ranges. Obvious constraints on the particle energies and angles involved are

$$E_3 \geq m_\pi \tag{3.24a}$$

$$E_4 \geq m_\pi \tag{3.24b}$$

$$E_5 \geq m_\pi \tag{3.24c}$$

$$\cos^2\Theta_3 \leq 1 \tag{3.24d}$$

$$\cos^2\Theta_4 \leq 1 \tag{3.24e}$$

$$\cos^2\varphi_{34} \leq 1. \tag{3.24f}$$

These constraints on the angles must be translated into conditions for t, u, x, and y, while an expression for $\cos\varphi_{34}$ can be obtained on inverting Eq.(3.7d) for w. Now, introducing the abbreviations

$$\tilde{t} = t - m^2 - m_\pi^2 \tag{3.25a}$$

$$\tilde{u} = u - m^2 - m_\pi^2 \tag{3.25b}$$

$$\tilde{x} = x - m^2 - m_\pi^2 \tag{3.25c}$$

$$\tilde{y} = y - m^2 - m_\pi^2 \tag{3.25d}$$

we can reexpress Eqs.(3.24a) and (3.24b) as

$$-\tilde{t} - \tilde{x} - 2m_\pi\sqrt{s} \geq 0 \tag{3.26}$$

$$-\tilde{u} - \tilde{y} - 2m_\pi\sqrt{s} \geq 0, \tag{3.27}$$

which follows on using the equations (3.8c) and (3.8d). The equation (3.24c), on the other hand, becomes

$$\sqrt{s} - E_3 - E_4 - m_\pi \geq 0, \tag{3.28}$$

on using the conservation of energy condition $E_3 + E_4 + E_5 = \sqrt{s}$ in the c.m. system. E_3 and E_4 can be eliminated from Eq.(3.28) using (3.8c) and (3.8d). Then it reads

$$\sqrt{s} + \frac{\tilde{t} + \tilde{x}}{2\sqrt{s}} + \frac{\tilde{u} + \tilde{y}}{2\sqrt{s}} - m_\pi \geq 0. \tag{3.29}$$

This expression can be further utilized to set an upper bound on either $\tilde{t} + \tilde{x}$ or $\tilde{u} + \tilde{y}$. Let us regard that for $\tilde{t} + \tilde{x}$. Eliminating $\tilde{u} + \tilde{y}$ using Eq.(3.27), Eq.(3.29) leads to the bound

$$\tilde{t} + \tilde{x} \geq -2s + 4\sqrt{s}m_\pi. \tag{3.30}$$

We next examine the angular condition Eq.(3.24d). In terms of t and x, or $\tilde{t}$ and $\tilde{x}$, this reads

$$\left(\frac{\tilde{t} - \tilde{x}}{4|\vec{p}_1||\vec{p}_3|}\right)^2 \leq 1, \tag{3.31}$$

where Eq.(3.8a) was used. By eliminating $4|\vec{p}_1|^2 = s - 4m^2$ and $|\vec{p}_3|^2 = E_3^2 - m_\pi^2$ with the aid of Eq.(3.8c), this condition becomes

$$(\tilde{t} - \tilde{x})^2 s \leq (s - 4m^2)((\tilde{t} + \tilde{x})^2 - 4sm_\pi^2). \tag{3.32}$$

In an analogous fashion, the angular condition Eq.(3.24e) can be rearranged to give a condition on $\tilde{u} - \tilde{y}$:

$$(\tilde{u} - \tilde{y})^2 s \leq (s - 4m^2)((\tilde{u} + \tilde{y})^2 - 4sm_\pi^2). \tag{3.33}$$

The final angular constraint, Eq.(3.24f) is rewritten in terms of the Mandelstam-like variables on considering Eq.(3.9), replacing w by $3m^2 + 3m_\pi^2 - s - x - y$ and the appropriate energies from Eqs.(3.8c) and (3.8d). This then takes the form

$$\frac{\left(s + \tilde{t} + \tilde{u} + \tilde{x} + \tilde{y} + m_\pi^2 + \alpha\gamma/s - \beta\delta/\tilde{s}\right)^2}{4(E_3^2 - m_\pi^2)(E_4^2 - m_\pi^2) - 2\delta(E_3^2 - m_\pi^2)/\tilde{s} - 2\beta(E_4^2 - m_\pi^2)/\tilde{s} + \beta^2\delta^2/\tilde{s}^2} \leq 1, \tag{3.34}$$

where the abbreviations

$$\alpha = \frac{\tilde{t} + \tilde{x}}{\sqrt{2}}, \qquad \beta = \frac{\tilde{t} - \tilde{x}}{\sqrt{2}}, \tag{3.35}$$

$$\gamma = \frac{\tilde{u} + \tilde{y}}{\sqrt{2}}, \qquad \delta = \frac{\tilde{u} - \tilde{y}}{\sqrt{2}} \tag{3.36}$$

have been introduced and $\tilde{s} = s - 4m^2$.

The integration region for the variables t, u x and y must be determined from the relations (3.26), (3.27), (3.30), (3.32), (3.33) and (3.34). From (3.26), it follows immediately that

$$\alpha \leq -\sqrt{2s}m_\pi, \tag{3.37}$$

while Eq.(3.32), considering the equal to sign, describes a hyperbola in the variables α and β with defining equation

$$\frac{\alpha^2}{2sm_\pi^2} - \frac{\beta^2}{2\tilde{s}m_\pi^2} = 1. \tag{3.38}$$

The hyperbola has semi-axes $a = \sqrt{2sm_\pi^2}$ and $b = \sqrt{2\tilde{s}m_\pi^2}$, and asymptotes $\beta = \pm b\alpha/a$. In view of Eq.(3.37), only the negative hyperbola must be considered, which is depicted in Fig. 8. In order to determine whether the integration region lies within or without this function, it suffices to choose a point in the plane. Choosing $\beta = 0$ and $\alpha < -a$ leads to the relations

$$E_3 = \frac{-\tilde{t} - \tilde{x}}{2\sqrt{s}} = -\frac{\alpha}{\sqrt{2s}} \tag{3.39}$$

$$2(\tilde{t} + \sqrt{s}E_3) = \sqrt{2}\beta = 0 \tag{3.40}$$

so that

$$(s - 4m^2)(E_3^2 - m_\pi^2) - (\tilde{t} + \sqrt{s}E_3)^2 > 0, \tag{3.41}$$

i.e. the condition Eq.(3.32) is fulfilled. The integration region thus lies within the hyperbola. The bound on $\tilde{t}+\tilde{x}$ that was found in Eq.(3.30) can be translated to the variable α and gives rise to the vertical line

$$\alpha \geq -\sqrt{2}s + 4\sqrt{\frac{s}{2}}m_\pi \tag{3.42}$$

shown in Fig. 7 with dots and which cuts off the integration regime to the left. This defines a clearly delineated area F_1 in the $\alpha - \beta$ plane for the integration region. Note that one could transform the conditions on α and β back to conditions on $\tilde{t}$ and $\tilde{x}$. This results in a hyperbola for these functions that is obtained on rotation of the α and β axes by $\pi/4$. It is not necessary to find this form explicitly, because the checks that are done to evaluate the integral will determine the range of integration numerically using the conditions on α and β.

In an analogous fashion, it is possible to construct an area F_2 in the variables $\gamma - \delta$ that are related to $\tilde{u}$ and $\tilde{y}$ that is delineated by the analogous condition

$$\gamma \geq -\sqrt{2}s + 4\sqrt{\frac{s}{2}}m_\pi \tag{3.43}$$

plus a hyperbola in the $\gamma - \delta$ plane. Taken together, these two areas $F_1 \times F_2$ span a superset of points in t-u-x-y space that constitute the region of integration, subject to the condition Eq.(3.34) being fulfilled.

IV. NUMERICAL CALCULATIONS

In this section, we examine the reaction $u\bar{u} \to \pi^+\pi^-\pi^0$. This particular process has been selected, because the analogous two particle final state hadronization process $u\bar{u} \to \pi^+\pi^-$ is the dominant channel [4] for $u\bar{u} \to MM'$, where M, M' are mesonic members of the $\mathrm{SU}_f(3)$ multiplet. In order to make a sensible comparison, we calculate the transition rate for this process, which is given in terms of the cross section $\sigma(s)$ as

$$\omega(s) = |\vec{v}_{rel}|\sigma(s), \tag{4.1}$$

where $\vec{v}_{rel}$ is the relative velocity of the incoming quarks, and which is given as

$$|\vec{v}_{rel}| = 2\sqrt{1 - \frac{4m^2}{s}} \tag{4.2}$$

in the centre of mass frame. Our numerical calculations are based on a Monte Carlo procedure for evaluating the fourfold integral in the expression Eq.(3.18) for the cross section. In implementing this, it proves useful to alter the integration region. As already mentioned, this consists of surfaces F_1 and F_2 in the α-β and γ-δ plane respectively and is bounded by the further condition Eq.(3.34). First we extend the surfaces F_1 and F_2 to the enlarged regions W_1 and W_2 that contain them, but which have simpler boundaries. The triangular region bounded by the asymptotes of the hyperbolae together with the vertical restriction on the value of the ordinate as indicated in Fig. 8 for the β-α plane is chosen as the extension of F_1 to W_1, and a similar construction is made for W_2 in the γ-δ plane. This has the advantage that random points can be chosen to be equally distributed in this triangular area for the Monte Carlo procedure. On actually performing the numerical integration, the caveat is imposed that the function to be integrated takes the required functional value in F_1, F_2 but which is zero otherwise, together with the restriction Eq.(3.34). The delineation of the integration regions for α and β is given via

$$\begin{aligned} -\alpha_{max} < \alpha < 0 \\ -\beta_{max} < \beta < \beta_{max} \end{aligned} \tag{4.3}$$

with $\alpha_{max} = 2/\sqrt{2} - \sqrt{s}/\sqrt{2}m_\pi$ and $\beta_{max} = \alpha_{max}\sqrt{\tilde{s}}/\sqrt{s}$.

In order to evaluate the transition rate, the individual contributions to $\mathcal{M}$ that occur in Eq.(2.42) must be specified. These are in turn dictated by the traces of the flavor factors, which sometimes vanish. For the specific combination of $\pi^+\pi^-\pi^0$ in the final state, the s-like channel contribution contains all six possible graphs,

$$\mathcal{M}^{s-\text{like}} = 2\mathcal{M}_\pi(p_3, p_4, p_5) + 2\mathcal{M}_\pi(p_4, p_5, p_3) + 2\mathcal{M}_\pi(p_5, p_3, p_4), \tag{4.4}$$

while in the t-like channel, only three possible graphs contribute,

$$\mathcal{M}^{t-\text{like}} = \mathcal{M}^{(t,w)} + \mathcal{M}^{(v,y)} + \mathcal{M}^{(t,y)}. \tag{4.5}$$

In the st-like channel, there are only four possibilities. Here the single outgoing meson must be a π^0, while the loop contains the π^+ and π^- outgoing in the final state. The two loop directions plus the attachment to either the incoming quark or antiquark line comprise these possibilites. They are fully summarized in the function

$$\mathcal{M}^{st-\text{like}} = \mathcal{M}^{(st)}(p_5). \tag{4.6}$$

Rather than evaluate the complete transition rate that is constructed from $\mathcal{M} = \mathcal{M}^{s-\text{like}} + \mathcal{M}^{t-\text{like}} + \mathcal{M}^{st-\text{like}}$, we evaluate first the transition rate in each particular channel, in order to illustrate the magnitude that each type of channel contributes. We comment briefly on our numerical procedure. In the s-like channel, the pseudoscalar polarization function $\Pi_{PS}(k^2)$ is required from Eq.(2.14), while for the st-like channel, the scalar polarization function $\Pi_S(k^2)$ enters as in Eq.(2.39), corresponding to the exchange of π or σ mesons respectively. At zero temperature, the case studied here, one has that at $k^2 = m_\pi^2$, the π is strongly bound, while at $k^2 = m_\sigma^2$, the σ is weakly unbound, since $m_\sigma^2 \simeq 4m^2 + m_\pi^2$. Thus the σ already has a small width, representing the unphysical decay into two quarks. At higher values of k^2, this unphysical width grows, and at large values of k^2, the pion can also develop a width. We have chosen to ignore such unphysical decays into quark constituents. This is done primarily for reasons of numerical simplicity – only the principle values of the integrals I_n that enter into $\Pi_{PS}(k^2)$ and $\Pi_S(k^2)$ are considered – and this allows one to focus on the role of the triangular vertex graphs, which are the physical cause of the decays into the mesons. This procedure simply assumes that the intermediate mesonic states are stable with regard to decay into their quark constituents, which is not unreasonable. Note that the imaginary parts of the I_n that

enter into the irreducible polarization functions commence always at the threshold $k^2 = 4m^2$. A detailed discussion of these functions giving their analytic structure, together with graphic illustrations as a function of k_0^2 and $\vec{k}^2$ can be found in Ref. [18].

For our numerical results, the parameters $\Lambda = 851$ MeV, $G\Lambda^2 = 2.87$, and $m_0 = 5.2$ MeV have been used. These lead to the values $f_\pi = 93$ MeV, $m_\pi = 135$ MeV and $\langle\bar{\psi}\psi\rangle = (-250 \text{ MeV})^3$. Calculated values of the quark mass yield $m = 265$ MeV and the pion quark coupling as being $g_{\pi qq} = 2.85$.

Figures 9,10, and 11 display the results for the s-like, t-like, and st-like channels individually. One sees that the st-like channel provides the largest yield, being substantially larger than the s-like channel (an order of magnitude) and the t-like channel (two orders of magnitude). Thus, one sees that within the set of graphs that are of the same order in the $1/N_c$ expansion in fact have a very different relevance. It is important to try to understand this, and we can do so on a heuristic level: one notes that both the s and st like channels contain a quark loop. The fewer the number of quark lines occurring in this loop, the more divergent, or less convergent this diagram will be. Graphs such as that occurring for the s-like channel contain a quark loop with four internal quark lines in contrast to the graphs of the st-like channel, which has a quark loop with three internal quark lines. One may thus expect that the st-like channel will dominate over the s channel. Our findings and this argument are in line with that of Ref. [9], in which all convergent terms are dropped and only the leading divergent or least convergent ones are retained. A similar argument was given in Ref. [10] for ignoring several $O(1/N_c)$ terms in the higher order corrections to the pion radius, in which the same argument was made on heuristic grounds. This numerical calculation now validates such heuristic claims. Thus this ordering plays an additional role in reordering the set of terms that occur beyond the $1/N_c$ expansion.

Obviously, by examining the graphs of Figs. 9 to 11, the full cross-section should be well approximated by that of the st-channel alone. This is given in Fig. 12, and includes the cross terms. We also compare our result with the transition rates for the processes $u\bar{u} \to \pi^+\pi^-$ and $u\bar{u} \to \pi^0\pi^0$ that proceed via the diagrams of Fig. 1. Here the process $u\bar{u} \to \pi^+\pi^-$ is the dominant one. We find, for the range of validity of the model, say $\sqrt{s} \leq 1$GeV, that the hadronization rate of u and $\bar{u}$ into three

pions, which is also driven by a two pion hadronization graph, is of the same order of magnitude as $u\bar{u}$ into two pions, despite the fact that the phase space is altered. This result indicates that transport or other models that include hadronization as a two meson level, require hadronization into at least three pions also.

V. SUMMARY AND CONCLUSIONS

In this paper, we have studied the three meson hadronization process $q\bar{q} \to MM'M''$ within the two flavor Nambu–Jona-Lasinio model. Our motivation stems from the fact that pions are light, almost massless particles and can thus be produced copiously. We have calculated transition rates for this process in order to assess the importance of this process in comparison with the standard binary processes that are usually input into transport models. Since the NJL model is currently under study as a transport model for a chiral theory [3,5,16], such questions can be answered within the context of the model itself. It has thus been our aim to investigate the transition rate for this process, in comparison with similar transition rates for two meson production $\bar{q} \to MM'$ for a specific initial state q and $\bar{q}$ being u and $\bar{u}$.

In our analytic discussion, we have found that there are three types of diagrams that contribute in the lowest level $1/N_c$ expansion that is appropriate to this model. Our numerical calculation however indicates that an additional criterion for deciding on which graphs dominate the set of diagrams in a particular $1/N_c$ class is the number of internal fermion lines when a fermion loop diagram is present. This criterion is in accord with the heuristic methods of Ref. [9], and which was used successfully in identifying the logarithmic contribution to the pion radius [10], and thereby recovering the known results of sigma models, other chiral models and chiral perturbation theory (CHPT) for this quantity. We have thus explicitly been able in this paper, to demonstrate that this crucial heuristic argument given in [10] is in fact valid, in particular in the context of a different calculation. In view of the fact that the dominance of the most divergent graph gives the expected result for the pion radius, our result here may not simply be a model artifact. We have at present no way of knowing how this result would compare with that calculated within another framework, say a confinement model [13] or within QCD itself, where the mechanism giving rise to the leading term may be different. We avoid any speculation here.

We conclude by stating that the numerical calculation shows that our results lie within the same order of magnitude as the hadronization rates for two pions, thereby indicating that such processes must necessarily be taken into account in hadronization at low energies.

VI. ACKNOWLEDGMENTS

We wish to thank our colleagues in the Institute for useful consversations, in particular, Hilmar Forkel. This work has been supported by the Deutsche Forschungsgemeinschaft DFG under the contract number Hu 233/4-4, and by the German Ministry for Education and Research (BMBF) under contract number 06 HD 742.

APPENDIX A: PAULI-VILLARS REGULARIZATION FOR THE INTEGRALS I_N

The evaluation of $I_n(a_1 \ldots, a_n)$ as defined in Eq.(2.19) is done using the Pauli-Villars regularization scheme. The reader is referred to one of the many papers involving such integrals for I_1 and I_2, see for example [8,17,18]. We simply quote the final results,

$$I_1 = -\frac{i}{(4\pi)^2}[m^2 \ln\left(1 - (\frac{\Lambda^2}{m^2+\Lambda^2})^2\right) + 2\Lambda^2 \ln\left(1 + \frac{\Lambda^2}{m^2+\Lambda^2}\right)]. \tag{A1}$$

and $I_2(p,0) = I_2(p)$ is

$$I_2(p) = -\frac{i}{(4\pi)^2}\sum_{j=0}^{2} C_j \int_0^1 dz \ln(m_j^2 - z(1-z)p^2). \tag{A2}$$

where $C_0 = 1$, $C_1 = 1$ and $C_2 = -2$ is a standard set of coefficients fulfilling $\sum_j C_j = \sum_j C_j m_j^2 = 0$. Here $m_j^2 = m^2 + \alpha_j^2 \Lambda^2$, with $\alpha_0 = 0$, $\alpha_1 = 2$ and $\alpha_2 = 1$. Reference [19] gives

$$I_3(p,k) = -\frac{i}{8\pi^2}\sum_{j=0}^{2} C_j \int_0^1 dyy \int_0^1 dx[\frac{1}{a^2 - b_j} + \frac{a^2 - b_j}{2(a^2-b_j)^2}], \tag{A3}$$

with $a = y(1-x)p + (1-y)k$ and $b_j = y(1-x)p^2 + (1-y)k^2 - m_j^2$, and

$$I_4(p,k,l) = -\frac{3i}{(4\pi)^2}\sum_{j=0}^{2} C_j \int_0^1 dzz \int_0^1 dy \int_0^1 dx x^2[-\frac{1}{4(a^2-b_j)^2} + \frac{a^2-b_j}{6(a^2-b_j)^3}], \tag{A4}$$

with $a = zx(1-y)p + x(1-z)k + (1-x)l$ and $b_j = zx(1-y)p^2 + x(1-z)k^2 + (1-x)l^2 - m_j^2$. An analytical expression for I_3 can be found in [19], while I_4 has been evaluated numerically.

APPENDIX B: MIXED TERMS IN THE SCATTERING AMPLITUDE

There are many mixed terms that occur between the various channels. Here we list only those that directly enter into the calculation of the transition rate for $u\bar{u} \to \pi^+\pi^-\pi^0$.

1. Mixed terms between t-like graphs

In this subsection, we list the cross terms that arise between t-like graphs in constructing the averaged matrix element, and which are required by virtue of Eq.(4.5). There are three such terms. The first of these is

$$\begin{aligned}\overline{\mathcal{M}^{(t,w)}\mathcal{M}^{(v,y)*}} = \frac{f_{t,w}f_{v,y}g_{\pi qq}^6}{4N_c}\Bigg\{&-\frac{1}{y-m^2} - \frac{1}{t-m^2} - \frac{(u-m^2)+(x-m^2)}{(v-m^2)(w-m^2)} \\ &+ \frac{(t-m^2)(x-m^2)}{(v-m^2)(w-m^2)(y-m^2)} + \frac{(u-m^2)(y-m^2)}{(t-m^2)(v-m^2)(w-m^2)} \\ &+ m_\pi^2\Bigg[\frac{3}{(v-m^2)(w-m^2)} + \frac{1}{(v-m^2)(y-m^2)} + \frac{1}{(t-m^2)(v-m^2)} \\ &+ \frac{-2(t-m^2)-(x-m^2)}{(v-m^2)(w-m^2)(y-m^2)} + \frac{y-x-2(u-m^2)}{(t-m^2)(v-m^2)(w-m^2)}\Bigg] \\ &+ m_\pi^6\frac{2}{(t-m^2)(v-m^2)(w-m^2)(y-m^2)}\Bigg\},\end{aligned} \tag{B1}$$

the second that is required is

$$\begin{aligned}\overline{\mathcal{M}^{(t,w)}\mathcal{M}^{(t,y)*}} = \frac{f_{t,w}f_{t,y}g_{\pi qq}^6}{4N_c}\Bigg\{&-\frac{2}{t-m^2} + \frac{(u-m^2)}{(t-m^2)(w-m^2)} \\ &+\frac{(v-m^2)}{(t-m^2)(y-m^2)} - \frac{(x-m^2)}{(w-m^2)(y-m^2)} \\ &+m_\pi^2\Bigg[-\frac{1}{(t-m^2)(w-m^2)} - \frac{1}{(t-m^2)(y-m^2)} + \frac{2}{(t-m^2)^2} \\ &+\frac{2}{(w-m^2)(y-m^2)} + \frac{(x-m^2)}{(t-m^2)(w-m^2)(y-m^2)}\Bigg] \\ &-m_\pi^6\frac{2}{(t-m^2)^2(w-m^2)(y-m^2)}\Bigg\}\end{aligned} \tag{B2}$$

and the last one is

$$\overline{\mathcal{M}^{(v,y)}\mathcal{M}^{(t,y)*}} = \frac{f_{v,y}f_{t,y}g_{\pi qq}^6}{4N_c}\left\{-\frac{2}{y-m^2}+\frac{(w-m^2)}{(t-m^2)(y-m^2)}\right.$$
$$+\frac{(x-m^2)}{(v-m^2)(y-m^2)}-\frac{(u-m^2)}{(t-m^2)(v-m^2)}$$
$$+m_\pi^2\left[\frac{2}{(y-m^2)^2}+\frac{1}{(t-m^2)(v-m^2)}+\frac{2u-w-x}{(t-m^2)(v-m^2)(y-m^2)}\right]$$
$$\left.-m_\pi^6\frac{2}{(t-m^2)(v-m^2)(y-m^2)^2}\right\}. \tag{B3}$$

2. Mixed terms between s-like graphs

Mixed terms between s-like graphs do not take a simple form in terms of the extended Mandelstam-like variables. Generally, one has

$$\mathcal{M}_\pi(p_a,p_b,p_c)\mathcal{M}_\pi^*(p'_a,p'_b,p'_c)$$
$$=8G^2g_{\pi qq}^2(N_f^j)^2\delta_{c_1c_2}\frac{|\bar{v}_2 i\gamma_5 u_1|^2 A_{\pi\pi\pi\pi}(p_a,p_b,p_c)A^*_{\pi\pi\pi\pi}(p'_a,p'_b,p'_c)}{|1-2G\Pi_{PS}(k^2)|^2}, \tag{B4}$$

where (p_a,p_b,p_c) or (p'_a,p'_b,p'_c) represent the combinations (p_3,p_4,p_5), (p_4,p_5,p_3) or (p_5,p_3,p_4). Averaging over incoming states and summing over final states leads to

$$\overline{\mathcal{M}_\pi(p_a,p_b,p_c)\mathcal{M}_\pi^*(p'_a,p'_b,p'_c)}$$
$$=\frac{2G^2g_{\pi qq}^6(N_f^j)^2}{N_c}\frac{4sA_{\pi\pi\pi\pi}(p_a,p_b,p_c)A^*_{\pi\pi\pi\pi}(p'_a,p'_b,p'_c)}{|1-2G\Pi_{PS}(k^2)|^2}, \tag{B5}$$

which is evaluated directly numerically.

3. Mixed terms between s-like and t-like graphs

Here three such products are required. The first of these is the averaged matrix element of $\mathcal{M}_\pi(p_a,p_b,p_c)$ together with its complex conjugate, which can be constructed as

$$\overline{\mathcal{M}_\pi(p_a,p_b,p_c)\mathcal{M}^{(t,w)*}}$$
$$=\frac{1}{N_c}\sum_{s_1,s_2}\bar{v}_2 i\gamma_5 u_1\frac{4iGg_{\pi qq}^3N_f^jA_{\pi\pi\pi\pi}(p_a,p_b,p_c)}{1-2G\Pi_{PS}(k^2)}\frac{-g_{\pi qq}^3f_{t,w}}{(t-m^2)(w-m^2)}$$
$$\times\bar{u}_1\gamma_5T_5(\not{p}_1-\not{p}_3+m)\gamma_5T_4(\not{p}_1-\not{p}_3-\not{p}_4+m)\gamma_5T_3v_2. \tag{B6}$$

Upon taking the traces and forming the complex conjugate, one finds the expression

$$\overline{\mathcal{M}_\pi(p_a,p_b,p_c)\mathcal{M}^{(t,w)*}}+\overline{\mathcal{M}^{(t,w)}\mathcal{M}^*_\pi(p_a,p_b,p_c)}=$$
$$-\frac{Gg^6_{\pi qq}f_{t,w}N_f^j}{N_c(t-m^2)(w-m^2)}2Re\left(\frac{A_{\pi\pi\pi\pi}(p_a,p_b,p_c)}{1-2G\Pi_{PS}(k^2)}\right)\{(v-m^2-m_\pi^2)(w-m^2-m_\pi^2)$$
$$(t-m^2-m_\pi^2)[(2(w-m^2)+(x-m^2-2m_\pi^2)-(u-m^2-m_\pi^2)(y-m^2-2m_\pi^2)\},\tag{B7}$$

and correspondingly

$$\overline{\mathcal{M}_\pi(p_a,p_b,p_c)\mathcal{M}^{(v,y)*}}+\overline{\mathcal{M}^{(v,y)}\mathcal{M}^*_\pi(p_a,p_b,p_c)}=$$
$$-\frac{Gg^6_{\pi qq}f_{v,y}N_f^j}{N_c(t-m^2)(w-m^2)}2Re\left(\frac{A_{\pi\pi\pi\pi}(p_a,p_b,p_c)}{1-2G\Pi_{PS}(k^2)}\right)\{(u-m^2-m_\pi^2)(y-m^2-m_\pi^2)$$
$$+(v-m^2-m_\pi^2)[(2(y-m^2)+(w-m^2-2m_\pi^2)]-(t-m^2-m_\pi^2)(x-m^2-2m_\pi^2)\},\tag{B8}$$

and

$$\overline{\mathcal{M}_\pi(p_a,p_b,p_c)\mathcal{M}^{(t,y)*}}+\overline{\mathcal{M}^{(t,y)}\mathcal{M}^*_\pi(p_a,p_b,p_c)}=$$
$$-\frac{Gg^6_{\pi qq}f_{v,y}N_f^j}{N_c(t-m^2)(y-m^2)}2Re\left(\frac{A_{\pi\pi\pi\pi}(p_a,p_b,p_c)}{1-2G\Pi_{PS}(k^2)}\right)\{(u-m^2-m_\pi^2)(y-m^2-m_\pi^2)$$
$$+(t-m^2-m_\pi^2)[(2(y-m^2)+(x-m^2-2m_\pi^2)]-(v-m^2-m_\pi^2)(w-m^2-2m_\pi^2)\}\tag{B9}$$

which ends this subsection.

4. Mixed terms between *st*-like and *t*-like graphs

Using the generic labels p_A, p_B and p_C to denote the outgoing pions in the t-like channel, one is required to form the cross term between the expression

$$\mathcal{M}^{t-\text{like}}=(ig_\pi)^2f\bar v(p_2)i\gamma_5\frac{i(\not p_C-\not p_2+m)}{(p_C-p_2)^2-m^2}i\gamma_5\frac{i(p_1-p_A+m)}{(p_1-p_A)^2-m^2}i\gamma_5u(p_1),\tag{B10}$$

where f is a flavor factor, and the expression for $\mathcal{M}^{st-\text{like}}$ in Eq.(2.40). The averaged cross product using the first term of Eq.(2.40) gives

$$\overline{\mathcal{M}_1^{(st)-\text{like}}\mathcal{M}^{t-\text{like}*}}=\frac{1}{4N_c}\frac{ig^4_{\pi qq}A_{\sigma\pi\pi}f}{(w-m^2)[(p_1-p_A)^2-m^2][(p_C-p_2)^2-m^2]}$$
$$\text{tr}_\gamma[(\not p_1+m)\gamma^5(\not p_1-\not p_A+m)\gamma^5(\not p_C-\not p_2+m)\gamma^5(\not p_2-m)\gamma^5(\not p_5-\not p_2+m)].\tag{B11}$$

The spinor trace can be performed, so that

$$\overline{\mathcal{M}_1^{(st)-\mathrm{like}}\mathcal{M}^{t-\mathrm{like}*}} = \frac{ig_{\pi qq}^4 A_{\sigma\pi\pi} fm}{N_c(w-m^2)} \frac{1}{[(p_1-p_A)^2-m^2][(p_C-p_2)^2-m^2]} \times[-(p_A\cdot p_C)p_5\cdot(p_1+p_2)+(p_A\cdot p_5)(p_1-p_2)\cdot p_C-(p_C\cdot p_5)p_A\cdot(p_1-p_2)]. \tag{B12}$$

Carrying out this procedure with the second term of Eq.(2.40) leads to precisely the same spinor trace, so that the expression differs only from the above in that $\omega - m^2$ is replaced by $v - m^2$, in building $\overline{\mathcal{M}_2^{(st)-\mathrm{like}}\mathcal{M}^{t-\mathrm{like}*}}$ and $\overline{\mathcal{M}^{(st)-\mathrm{like}}\mathcal{M}^{t-\mathrm{like}*}} = \overline{\mathcal{M}_1^{(st)-\mathrm{like}}\mathcal{M}^{t-\mathrm{like}*} + \mathcal{M}_2^{(st)-\mathrm{like}}\mathcal{M}^{t-\mathrm{like}*}}$.

When the incoming states are u and $\bar{u}$, and the outgoing states $\pi^+\pi^-\pi^0$, three t-like graphs can be constructed in which the outgoing momenta are permuted. These cases are (a) $p_A = p_5 = p_{\pi^0}$, $p_B = p_3 = p_{\pi^+}$ and $p_C = p_4 = p_{\pi^-}$ with $f = 2$; (b) $p_A = p_3 = p_{\pi^+}$, $p_B = p_5 = p_{\pi^0}$ and $p_C = p_4 = p_{\pi^-}$ with $f = -2$, and (c) $p_A = p_3 = p_{\pi^+}$, $p_A = p_4 = p_{\pi^-}$ and $p_C = p_5 = p_{\pi^0}$ with $f = 2$. Combining these three contributions and moving to the extended Mandelstam variables, one finds the form

$$\begin{aligned}\overline{\mathcal{M}^{(st)-\mathrm{like}}\mathcal{M}^{t-\mathrm{like}*}} = {} & \frac{img_{\pi qq}^4 A_{\sigma\pi\pi}}{N_c}\left[\frac{1}{w-m^2}+\frac{1}{v-m^2}\right] \\ & \times [\frac{v-m^2)((x-u-v-m^2)-m_\pi^2(x-y-v-m^2)}{[v-m^2][y-m^2]} \\ & + \frac{(w-m^2)(v-y)-(v-m^2)(t-m^2)-m_\pi^2(w-t-u+m^2)}{[t-m^2][y-m^2]} \\ & + \frac{(w-m^2)(y-t-v+m^2)-m_\pi^2(u-v-t+m^2)}{[t-m^2][w-m^2]}]\end{aligned} \tag{B13}$$

in total. The mixed term between the (st)-like and s-like graphs does not have a simple form, and must be constructed from Eq.(2.40) and Eq.(2.28).

REFERENCES

[1] Y. Nambu and G. Jona-Lasinio, Phys. Rev. **122** (1961), 345; **124** (1961), 246.

[2] For reviews, see U. Vogl and W. Weise, Prog. Part. Nucl. Phys. **27** (1991), 195; S.P. Klevansky, Rev. Mod. Phys. **64** (1992), 649; T. Hatsuda and T. Kunihiro, Phys. Rep. **247** (1994), 241; C.V. Christov et al., Prog. Part. Nucl. Phys. **37** (1996) 91; R. Alkofer, H. Reinhardt and H. Weigel, Phys. Rep. **265** (1996) 139.

[3] S.P. Klevansky, A. Ogura and J. Hüfner, Ann. Phys. (N.Y.) **261** (1997) 37.

[4] P. Rehberg, S.P. Klevansky and J. Hüfner, Phys. Rev. **C53** (1996) 410.

[5] A. Abada and J. Aichelin, Phys. Rev. Lett. **74** (1995) 3130; L. Bot and J. Aichelin, J. Phys. **G23** (1997) 1947.

[6] P. Rehberg and J. Hüfner, hep-ph/9708460, Nucl. Phys., to appear.

[7] E. Quack and S.P. Klevansky, Phys. Rev. **C 49** (1994), 3283.

[8] V. Dmitrašinović, H.J. Schulze, R. Tegen and R.H. Lemmer, Ann. Phys. (N.Y.) **238** (1995), 332.

[9] T. Eguchi, Phys. Rev. **D14** (1974) 2755; T Eguchi and H. Sugawara, Phys. Rev. **D10** (1974) 4257.

[10] H.-J. Hippe and S.P. Klevansky, Phys. Rev. **C52** (1995) 2172.

[11] R. Tarrach, Z. Phys. **C2** (1974) 221.

[12] J. Gasser and H. Leutwyler, Ann. Phys. (N.Y.) **158** (1982) 142.

[13] R. Alkofer and A. Bender, Int. J. Mod. Phys. **A10** (1995) 3319.

[14] E. Byckling and K. Kajantie. *Particle Kinematics*, (John Wiley and Sons, 1973).

[15] C. Itzykson and J.-B. Zuber, *Quantum Field Theory*, (McGraw-Hill, 1980).

[16] C. Spieles, H. Stöcker and C. Greiner, Phys. Rev. **C57** (1998) 908.

[17] P. Piwnicki, S.P. Klevansky and P. Rehberg, Phys. Rev. **C 58** (1998) 502 .

[18] P. Rehberg and S.P. Klevansky, Ann. Phys. (N.Y.) **252** (1996) 422.

[19] G. 't Hooft and M. Veltman, Nucl. Phys. **B153** (1979) 365.

FIGURE CAPTIONS.

FIG.1: s, t and u channel graphs available for the hadronization of $q\bar{q} \to MM'$, to lowest order in the $1/N_c$ expansion.

FIG.2: s-like, t-like and st-like channels available for the hadronization of $q\bar{q} \to MM'M''$, to lowest order in the $1/N_c$ expansion.

FIG.3: Exchange graph in the s-like channel, for $q\bar{q} \to MM'M''$.

FIG.4: Vertex associated with the s-like channel hadronization graph.

FIG.5: The vertex $\pi \to \pi\pi\pi$ cross channels obtained by permutations of the external meson indices.

FIG.6: Six available t-like channels.

FIG.7: Two particle production from an intermediate state.

FIG.8: Region of integration in the α-β plane. The solid line indicates the negative hyperbola that is determined by Eq.(3.38). The dotted vertical line is the boundary given by Eq.(3.42). The asymptotes of the hyperbola are indicated by the dashed line. The surface F_1 is bounded to the left of the solid line and the right of the dotted vertical line. W_1 is the triangle bounded to the right by the dotted vertical line and to the left by the dashed lines.

FIG.9: Transition rate ω plotted as a function of $\sqrt{s}$ for the s-like channel.

FIG.10: Transition rate ω plotted as a function of $\sqrt{s}$ for the t-like channel.

FIG.11: Transition rate ω plotted as a function of $\sqrt{s}$ for the st-like channel.

FIG.12: Transition rate ω plotted as a function of $\sqrt{s}$.

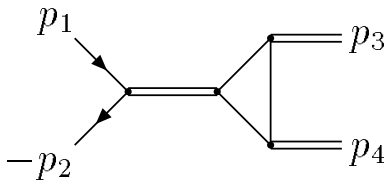

s channel

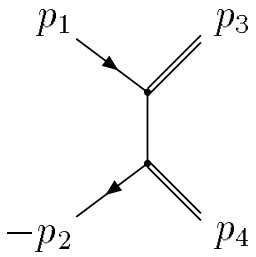

t channel

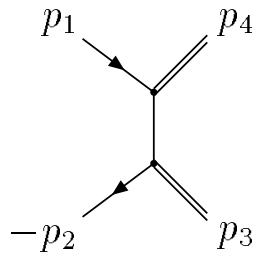

u channel

Figure 1

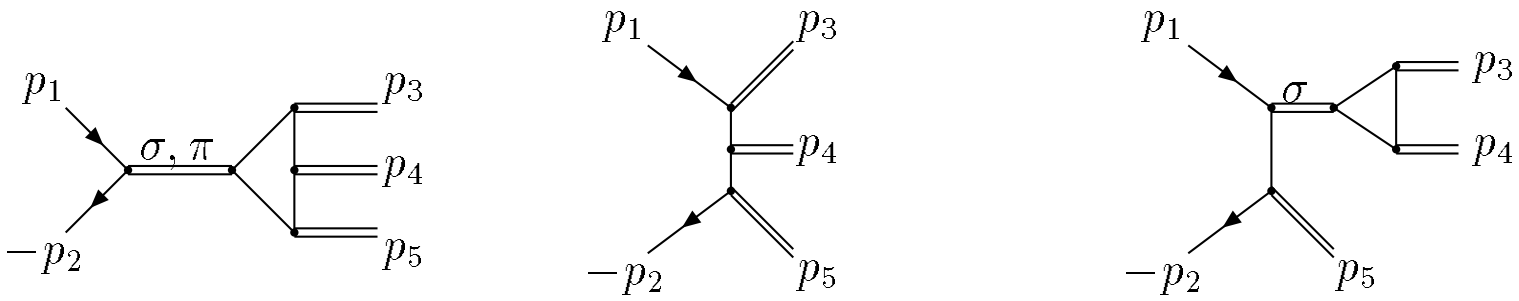
p_1
σ, π
p_3
p_4
p_5
$-p_2$
s-like channel
p_1
p_3
p_4
$-p_2$
p_5
t-like channel
p_1
σ
p_3
p_4
$-p_2$
p_5
st-like channel

Figure 2

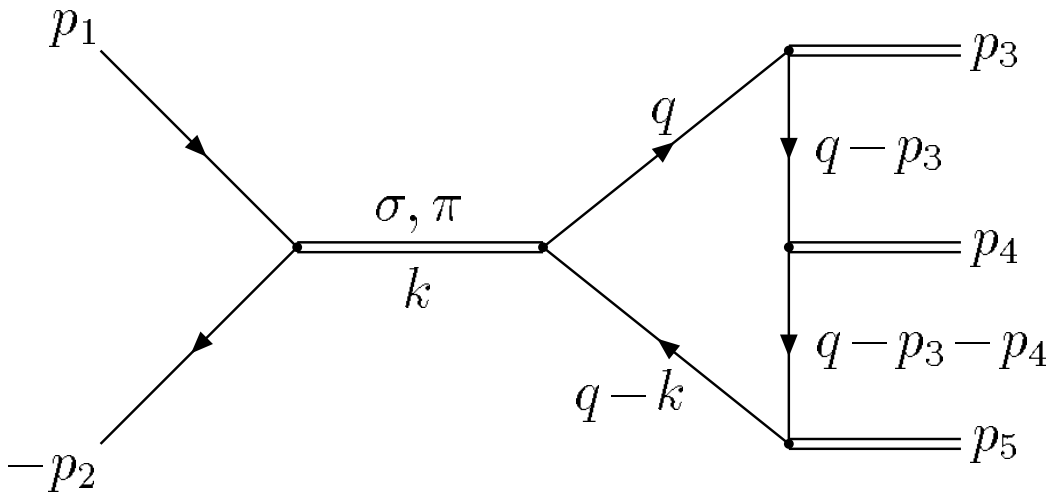

Figure 3

Figure 4

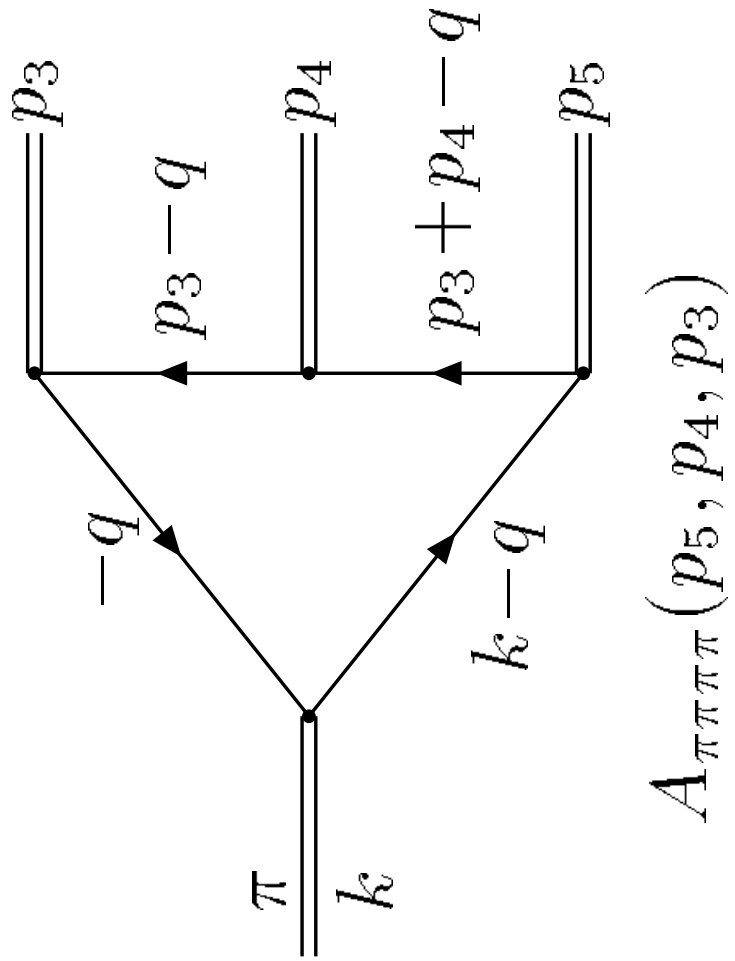

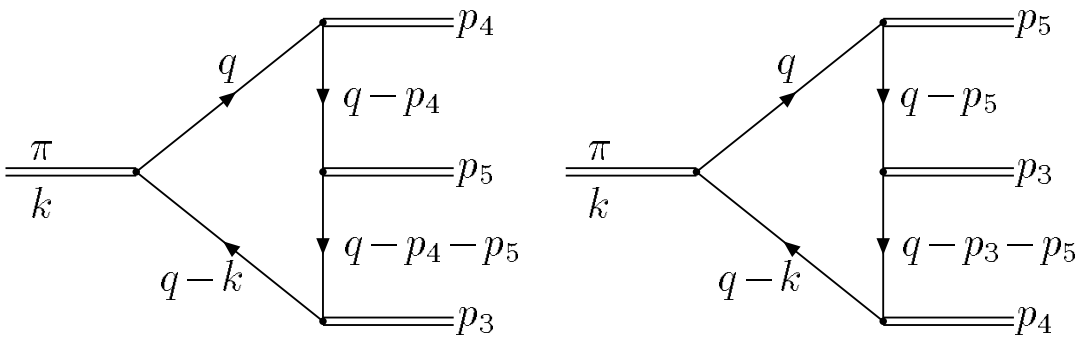
p_4
q
$q-p_4$
π
k
p_5
$q-p_4-p_5$
$q-k$
p_3
a) $A_{\pi\pi\pi\pi}(p_4,p_5,p_3)$
p_5
q
$q-p_5$
π
k
p_3
$q-p_3-p_5$
$q-k$
p_4
b) $A_{\pi\pi\pi\pi}(p_5,p_3,p_4)$

Figure 5

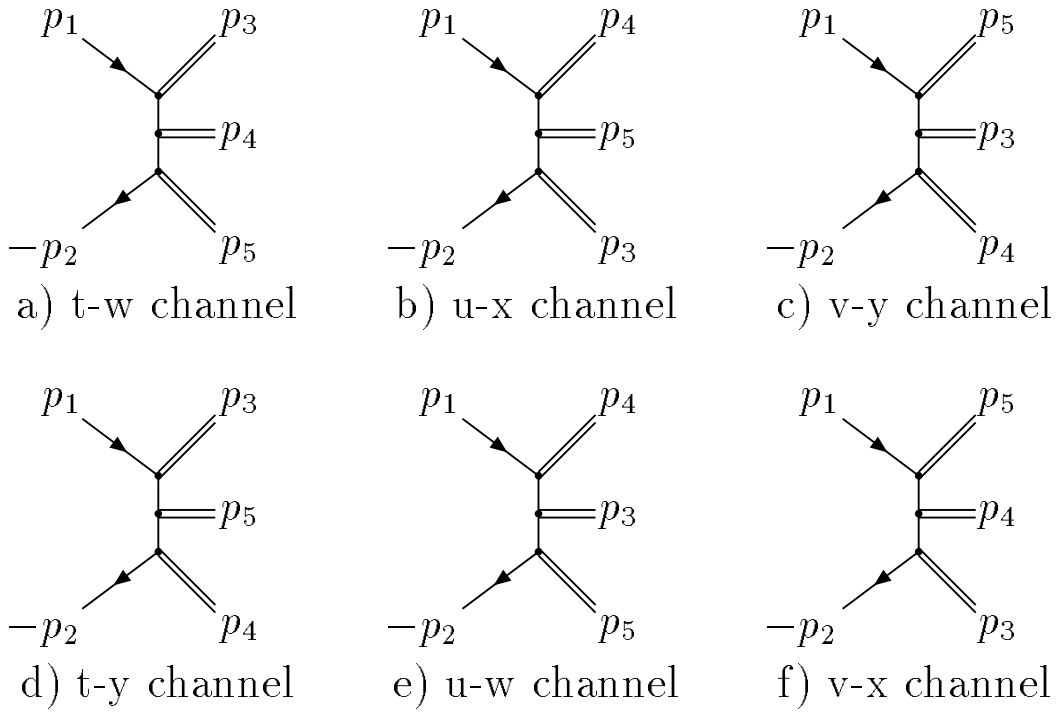
p_1
p_3
p_4
$-p_2$
p_5
a) t-w channel
p_1
p_4
p_5
$-p_2$
p_3
b) u-x channel
p_1
p_5
p_3
$-p_2$
p_4
c) v-y channel
p_1
p_3
p_5
$-p_2$
p_4
d) t-y channel
p_1
p_4
p_3
$-p_2$
p_5
e) u-w channel
p_1
p_5
p_4
$-p_2$
p_3
f) v-x channel

Figure 6

Figure 7

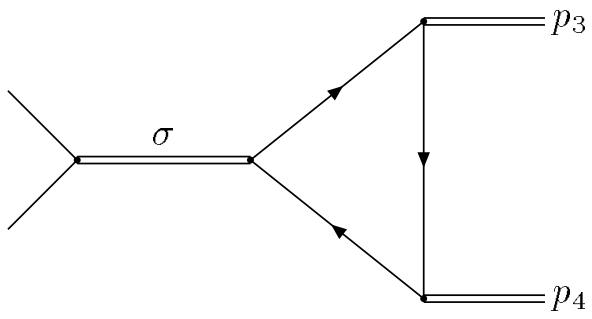

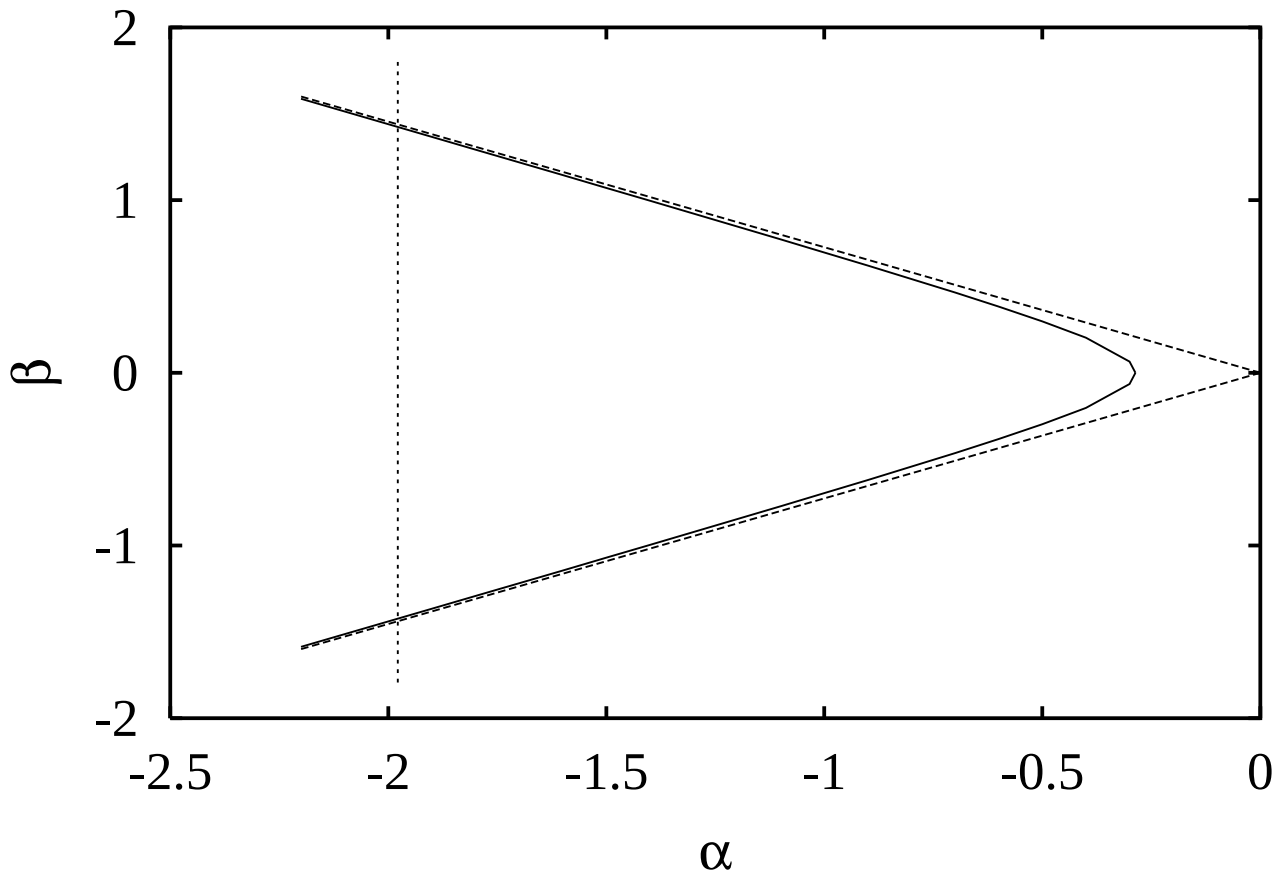

Figure 8

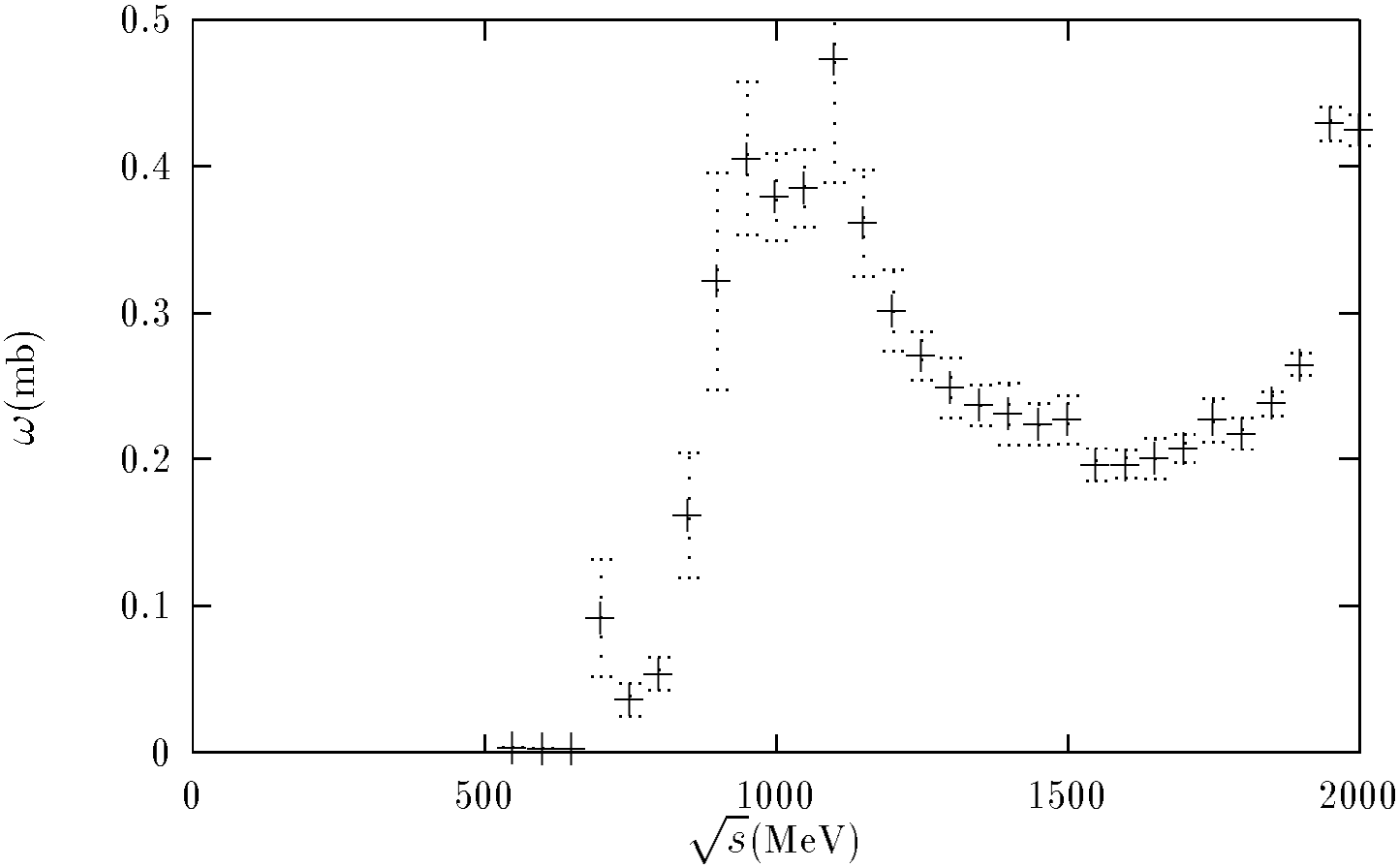

Figure 9

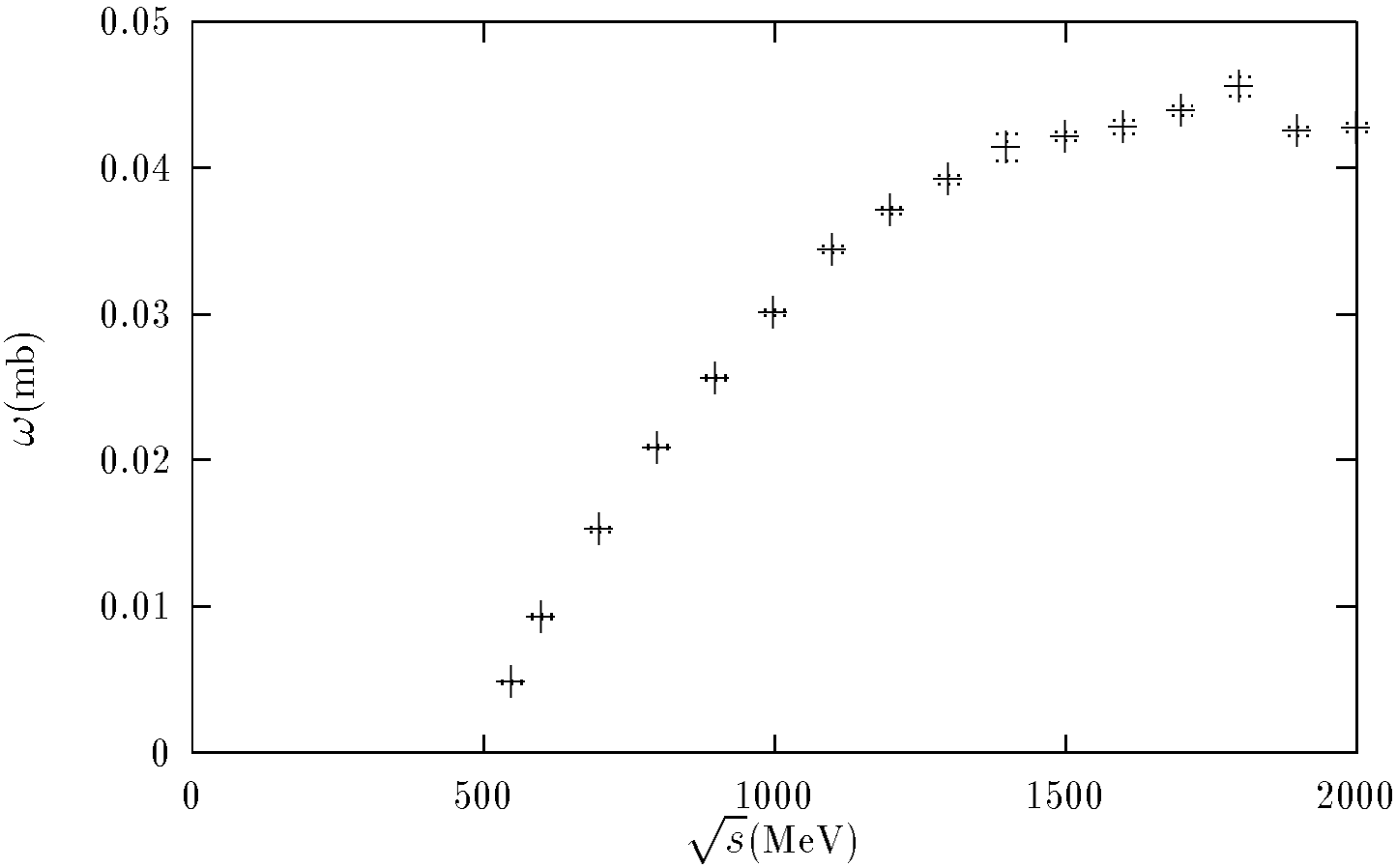

Figure 10

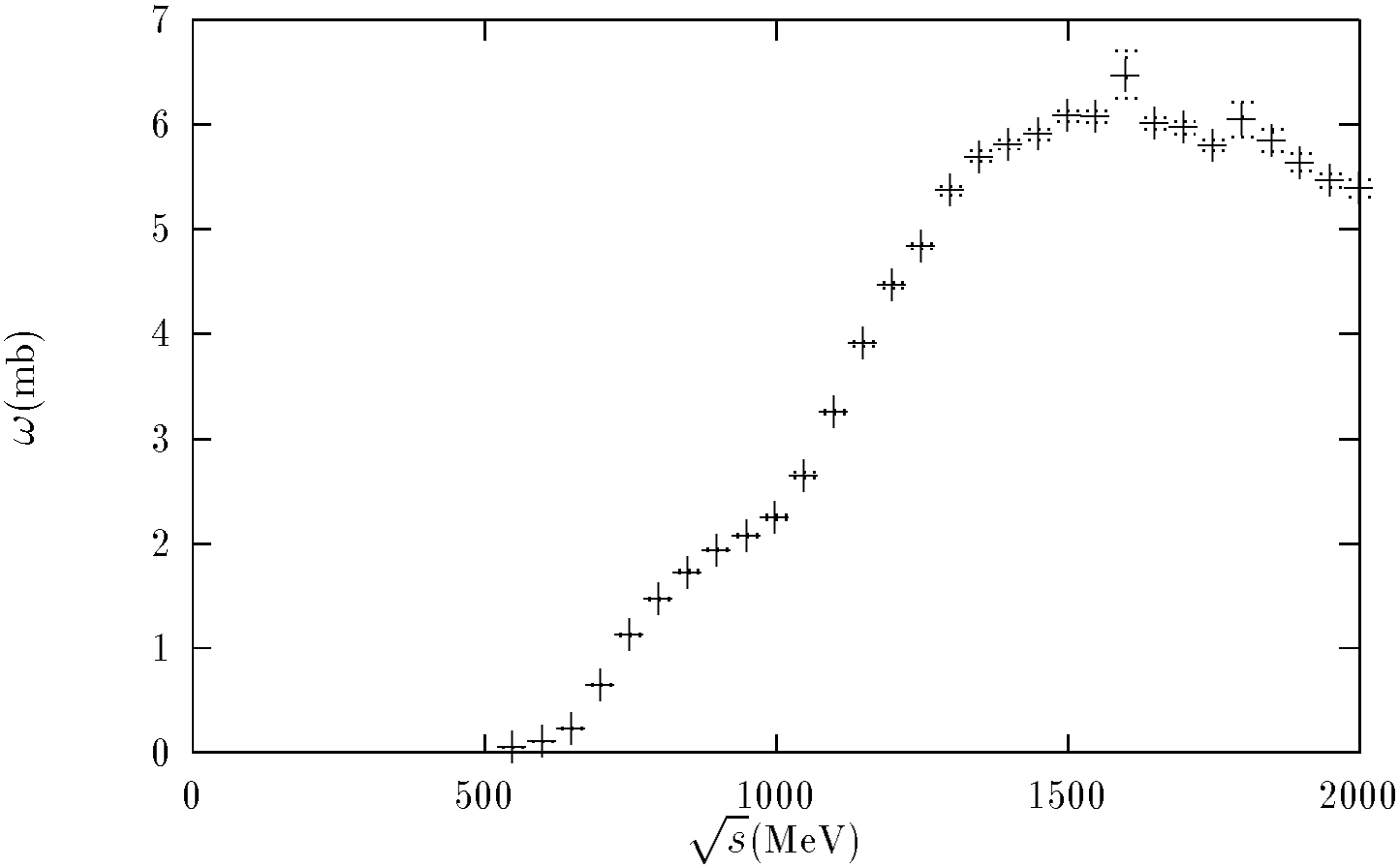

Figure 11

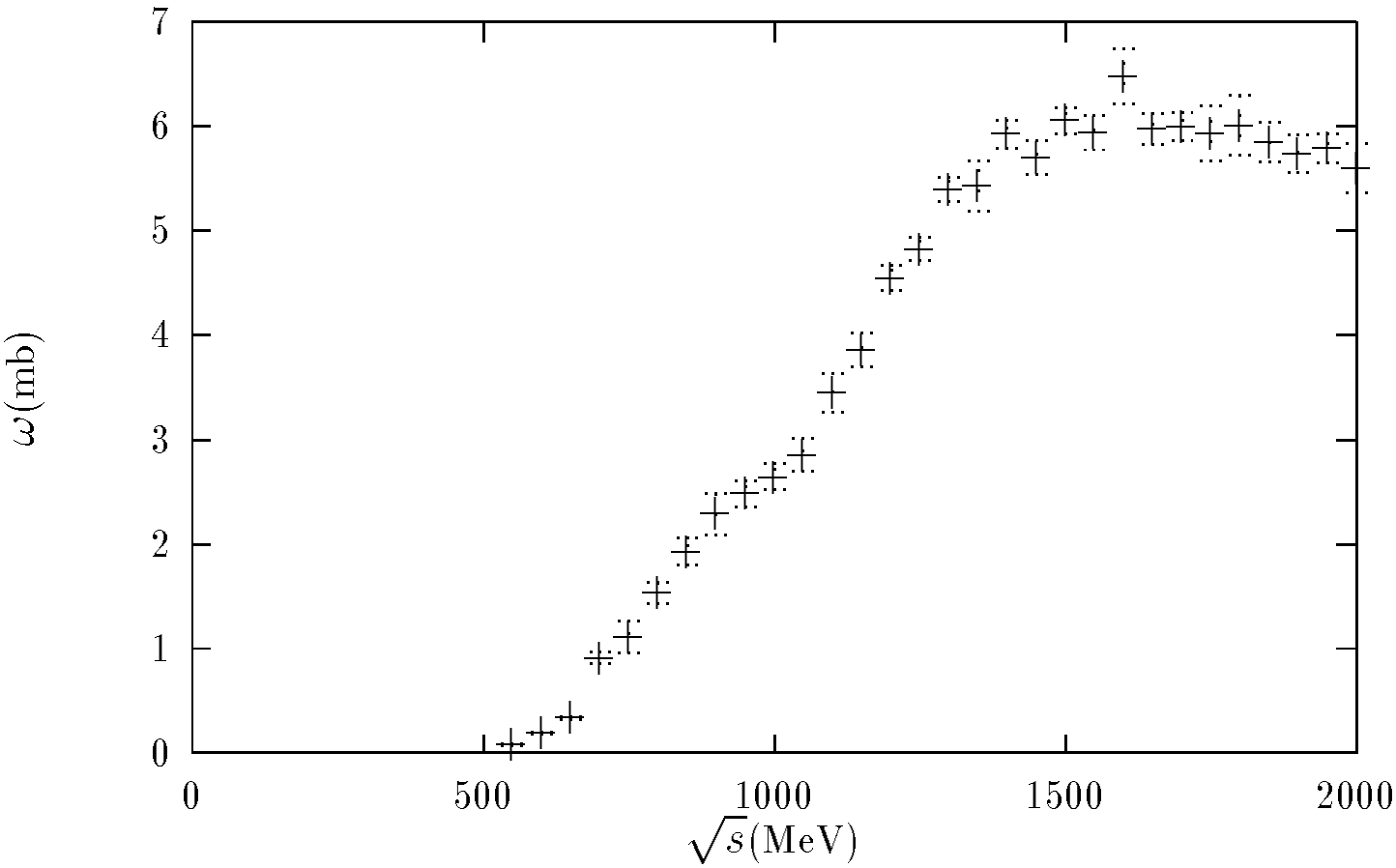

Figure 12